2

Some Contemporary and Prospective Applications of High Temperature Superconductors

Z. Güven Özdemir[1], Ö. Aslan Çataltepe[2] and Ü. Onbaşlı[3]
[1]*Yıldız Technical University, Physics Department, Davutpaşa Cad. Esenler, İstanbul, 34210*
[2]*Anatürkler Educational Consultancy & Trading Company, Cemil Topuzlu Cad. Üçem Konak No:73 D:1 Göztepe,Kadıköy*
[3]*Marmara University, Physics Department, Rıdvan Paşa Cad. 3. Sok. 4/12 Göztepe, Istanbul, Turkey*

1. Introduction

High temperature superconductors (HTS) have a wide range of very sensitive and reliable advanced technological applications. In this chapter, some examples of contemporary and prospective usage of the superconductors such as in vivo living body measurements in medicine, terahertz equipments for security systems, quantum bit namely "qubit" applications in quantum computation and bolometers for some space investigations will be dealt with.

Especially in medicine, superconductors have been reliably utilized in Magnetic Resonance Imaging (MRI), Magnetic Resonance Spectroscopy (MRS), magnetoencephalography (MEG) and magnetocardiography (MCG) for both analysis of magnetic activity of different regions of the human body such as brain and heart's wave activities and very early diagnosis of several diseases. All equipments mentioned above contain Superconducting Quantum Interference Device (SQUID), which is based on the Josephson Effect. SQUID is a very sensitive magnetic detector to determine the change of the magnetic flux in material media of the order of 10^{-15} Tm^2, which coincides with the order of magnetic flux quanta, $\Phi_0 = 2.0678x10^{-15}\ Tm^2$. The sensitivity of SQUID is revealed easily by remembering the fact that the magnetic field of the Earth equals to $5x10^{-5}$ Tesla.

Besides these contemporary applications in medicine mentioned above, the Proton-MRS (P-MRS) measurements will be proposed for forensic science investigations as one of the prospective implementations of HTS's. Because of the fact that some in vivo investigations via P-MRS provide the facility to detect the minor changes of metabolites in human brain (Onbaşlı et al., 1999), the method, which enables to detect the mild head injuries, which cannot be recognized according to Glasgow Coma Scale (GCS) (Teasdale & Jennett, 1974) from the neurological point of view, will be presented in this chapter.

Moreover, one of the remarkable features of HTS is that some oxide layered HTS work as a terahertz wave source. From this point of view, HTS's are also utilized in security systems, in remote sensing and non-destructive diagnosis. As was previously determined that the

mercury based copper oxide layered HTS (mercury cuprates) act as a natural terahertz wave cavity at particular temperature interval (Özdemir et al., 2006; Güven Özdemir et al., 2009). Hence, some part of the chapter will be related to the investigation of the terahertz emission of the superconductor mentioned.

The last part of the chapter will be related to the facility of prospective application of the mercury cuprates as a quantum bit, "qubit" in particular flux qubit (Güven Özdemir, 2011), which is based on the occurrence of the two fluxoid states with equal energy but opposite circulating current at the same time in the system (Mooij et al., 1999). As is known, qubits are fundamentally considered as the main building block of both quantum computation, quantum communication etc. In recent years, quantum computers, which are based on qubit operations, have an increasing attention due to their both high speed and memory capacity. In the present superconducting qubit technology, some low temperature superconductors especially aluminum thin film superconductors have been extensively utilized. In this context, for a prospective usage of HTS, mercury cuprates as one of the oxide layered high temperature superconductors will be proposed as an intrinsic flux qubit in this chapter.

2. Clinical usage of Superconducting Quantum Interference Device (SQUID)

The superconducting magnets in ultra sensitive magnetic detectors (1.5 Tesla and above) namely SQUID magnetometer (Superconducting Quantum Interference Device) implement the reliable observation of the metabolites in the living organisms for the clinical applications.

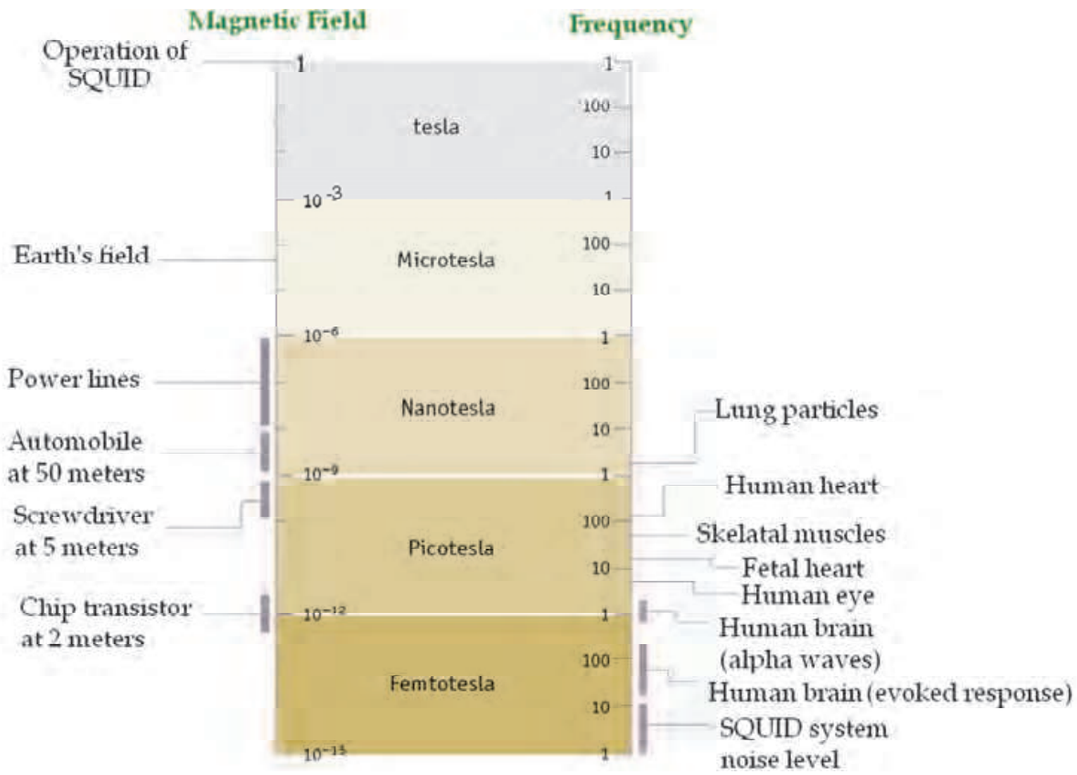

Fig. 1. Magnitudes of some biomagnetic fields (Fishbine, 2003).

As is known, the functions of human body are realized by the displacement of ions such as Na^+, K^+, Cl^- etc. The displacement of the ions corresponds to a current which produces a magnetic field. In Figure 1, the magnitudes of biomagnetic fields together with the other magnetic field sources are given.

According to Figure 1, especially biomagnetic fields produced by neuron cells' activities are very weak. They have magnetic field strengths of fT (femtoTesla i.e. 10^{-15}T). For comparison, the Earth's magnetic field is measured in micro Tesla and a magnetic resonance imaging system operates at several Tesla. The detection of such very small magnetic fields reliably is realized by the most sensitive magnetic field detector known as Superconducting Quantum Interference Device, namely SQUID.

A SQUID uses the properties of electron-pair wave coherence and Josephson Effect to detect very small magnetic fields. For example, to measure the magnetic field, that is produced by the electrical activity in brain, a special non-invasive imaging technique namely Magnetoencephalography (MEG), which contains SQUID sensors, are used (Fishbine, 2003).

In Figure 2, the representative illustration of detection of physical activities in human brain by MEG is given. The accuracy of measuring brain waves by MEG depends on the magnetic shielding of SQUID sensors from ambient magnetic fields such as the magnetic field of the Earth, power line's magnetic field and etc.

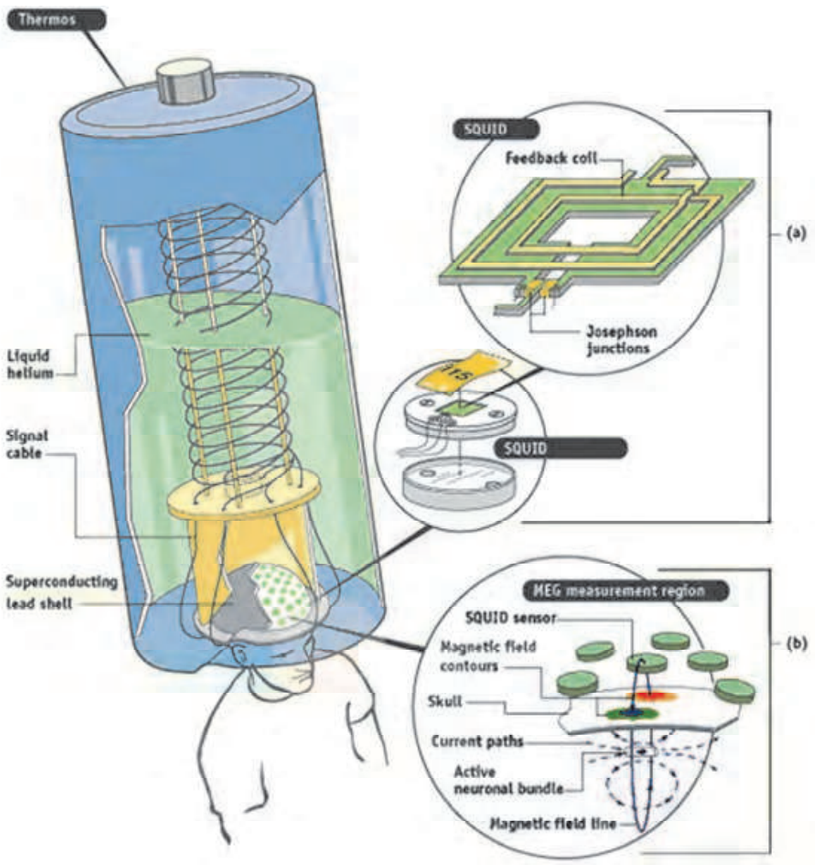

Fig. 2. Representative illustration of detection of physical activities in human brain by MEG (Fishbine, 2003).

As it is seen from Figure 2, SQUID sensors and the superconducting lead shell are cooled by immersion in liquid helium. In the superconducting state, lead shell expels ambient magnetic fields at all frequencies and hence it is ensured that SQUID sensor is only detect the magnetic field generated by brain waves. Each SQUID sensor contains a coil of superconducting wire that receives the brain fields and is magnetically coupled to the SQUID, which produces a voltage proportional to the magnetic field received by the coil. A computer program converts the SQUID data into maps of the currents flowing throughout the brain as a function of time (Fishbine, 2003).

2.1 Proton Magnetic Resonance Imaging (P-MRI) for medical diagnosis

Approximately 80% of human body is composed of water molecules and each water molecule consists of two hydrogen nuclei i.e. protons. In P-MRI measurements, the nuclear spins of hydrogen nuclei are aligned in one direction by applying strong magnetic fields of 1.5-3T that are generated by superconducting magnets. Afterwards, the polarized spins in one direction are excited by properly tuned radio frequency radiation. When the influence of short pulse of radio waves is removed, they drift back to their initial position, thereby

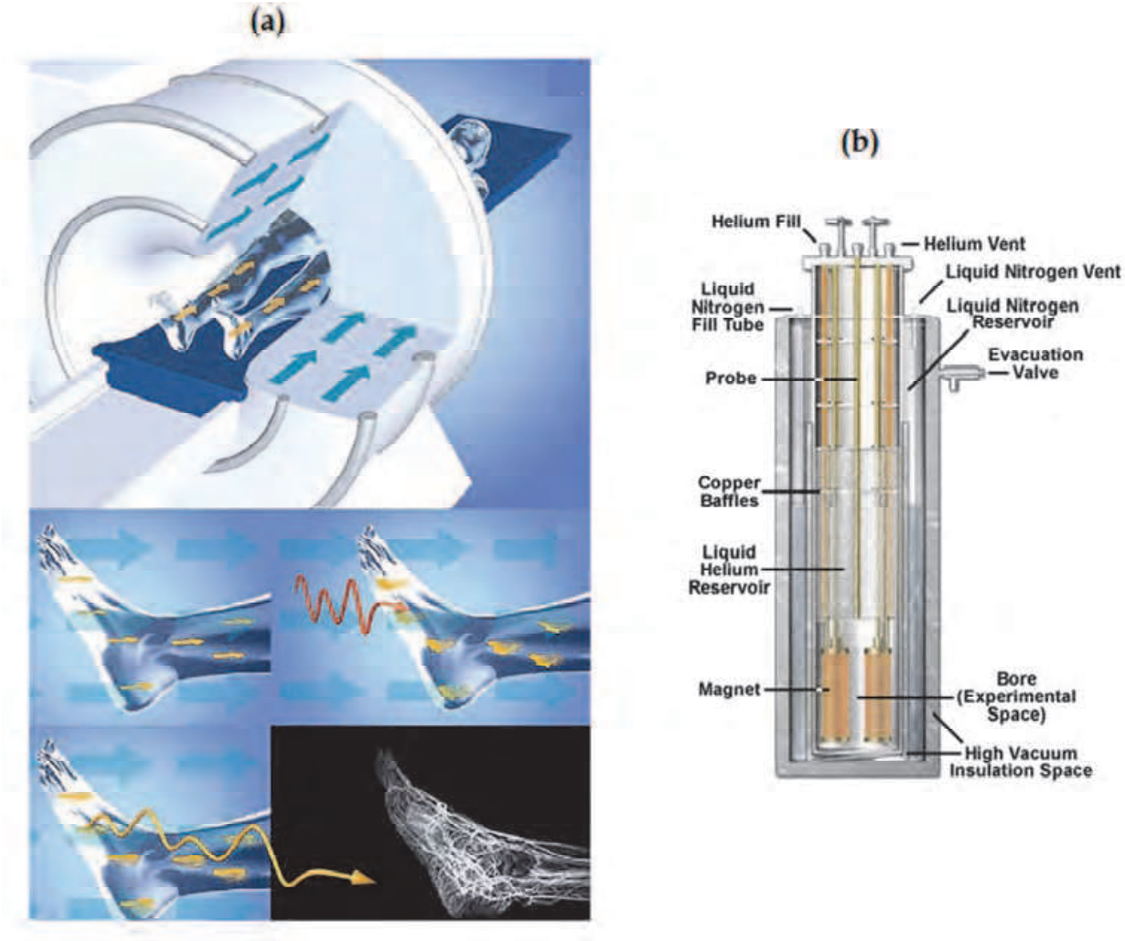

Fig. 3. (a) The working principle of P-MRI (Bayer, 2010). (b) The schema of superconducting magnets (National High Magnetic Field Laboratory, FSU, 2010).

emitting electromagnetic signals that can be used to reconstruct an image of the inside of the body. The protons in different tissues of the body (e.g. fat, muscle and etc.) realign at different speeds, so that the different structures of the body can be revealed (Georgia State University, 2010; Wikipedia, 2010; Bayer, 2010). The main steps of P-MRI are given in Figure 3(a).

The MRI technique has been extensively used for especially imaging the brain, heart, muscles and joints, for early diagnosis of cancer cells.

Superconducting magnets have a crucial role in P-MRI measurements. A superconducting magnet is an electromagnet made from coils of superconducting wire. Superconducting magnets can produce stronger and homogeneous magnetic fields than iron-core magnets. The most remarkable feature of the superconducting magnets is their capability of supporting very high current density with a vanishingly small resistance.

In conventional MRI devices, low temperature type II superconductors such as NbTi alloy are used to make coil windings for superconducting magnets. The illustration of typical superconducting magnet is shown in Figure 3(b).

Although, superconducting magnets are relatively more expensive to be build than ordinary iron-core magnets and require a constant supply of liquid helium closed cycle system, superconducting magnets have great advantages to detect very weak signals come from different sections of brain. If an ordinary magnet is used in MRS, only a giant water peak is observed, since approximately 80% of the tissue investigated consists of water molecule. Usage of superconducting magnet, which generates strong magnetic fields of 1,5-3T, enables both to suppress the signal comes from water molecules and distinguish the very weak signals, which have slightly different frequencies and that come from different metabolites secreted at the vicinity of the related tissue (Salibi & Brown, 1998).

2.2 Proton Magnetic Resonance Spectroscopy (P-MRS)

P-MRS generally produces spectra via Fourier transformation process of the tissue investigated instead of creating an image of the tissue. In vivo P-MRS, an appropriate radio frequency is applied the tissue and the signal comes from the tissue is measured and the

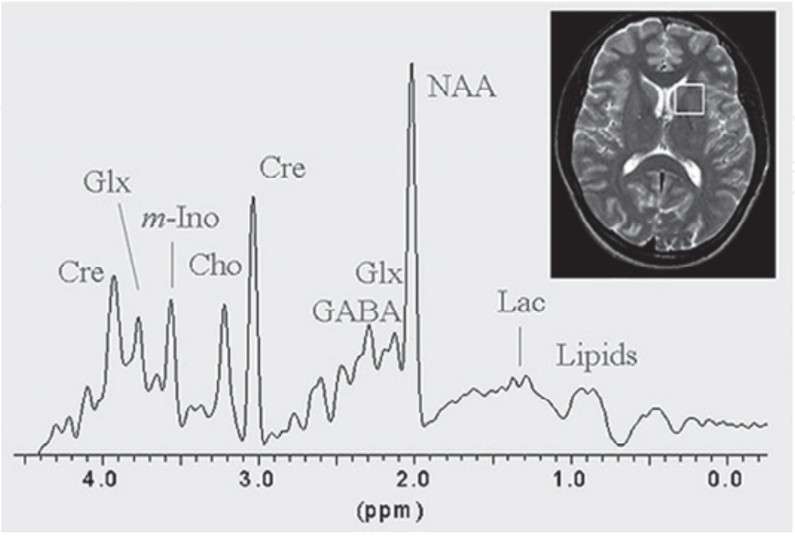

Fig. 4. P-MRS results of healthy human brain by means of metabolites. (Blamire, 2010)

Fourier transformation technique is used. In vivo P-MRS use position, signal intensity and line width along with spectral patterns to display chemical information about the related metabolites. A "ppm i.e. parts per million" scale describes the position of the peaks or resonances on the x-axis. Each peak in the spectrum arises from different brain metabolites. The heights of the peaks in the vertical axis refer to the concentrations of metabolites in arbitrary intensity scale.

In Figure 4, the proton magnetic resonance spectroscopic curve of a healthy human brain tissue with N-acetylaspartate (NAA), creatine (Cr), cholin (Cho) and etc. metabolite peaks is shown. Some of the metabolite peaks appear at the specific ppm value in the x-axis of the spectroscopic data. For example NAA peak appears at 2.0 ppm and NAA is accepted as the neural marker. While the primary resonance of Cr lies at 3.03 ppm, Cho resonates at 3.2 ppm (Danielsen &Ross, 1999; Blamire, 2010; Frahm et al., 1989).

2.3 *In vivo* experimental detection of Mild Traumatic Brain Injury (MTBI) by means of Proton Magnetic Resonance Imaging (P-MRI) and Proton Magnetic Resonance Spectroscopy (P-MRS)

In this chapter, we will focus on the detection of mild traumatic brain injuries (MTBI) by means of both Proton Magnetic Resonance Imaging (P-MRI) and Proton Magnetic Resonance Spectroscopy (P-MRS) techniques based on our experimental investigations. Although, the physical principle of both neuro-imaging techniques are the same, the information comes from these methods are completely different. Whereas the magnetic interaction between applied magnetic field and hydrogen nuclei is considered for P-MRI, the detection of chemical variation at the vicinity of hydrogen nuclei is realized in P-MRS. The main goal of this section is to determine mild traumatic brain injury (MTBI) at which no significant pathology is seen by imaging studies and that is considered as healthy based upon the Glasgow Coma Score (GCS).

As is known, a neurological GCS, which was published in 1974 (Teasdale & Jennett, 1974), aims to give a reliable information about the status of the central nervous system in three types of tests: eye, verbal and motor responses of the patient. The GCS is given in Table 1.

In GCS, the sum of the value that is related to the three types of tests (eye, verbal and motor) is used to assess the level of consciousness after head injury. According to the values in Table 1, while "the lowest possible score of 3" corresponds to the deep coma or death, "the highest score of 15" indicates the fully awake person.

Generally brain injuries are classified as severe with GCS ≤ 8, moderate with CGS:9-12 and minor GCS ≥ 13.

In MTBI, often no lesion or a few numbers of lesions are detected by MRI findings so that in many cases neuoro-imaging findings do not completely explain the clinical symptoms. In this context, P-MRS is commonly used for in vivo detection of variation of the quantity of metabolites in brain (Ariza et al., 2004; Govindaraju et al., 2004). P-MRS is a very sensitive and noninvasive in vivo technique to assess the metabolic status of brain which can quantify selected cerebral metabolites including N-acetylaspartate (NAA), a marker of neuronal and axonal viability (Bachelard & Badar-Goffer, 1993), total creatine (Cr), which reflects energy status, total choline (Cho) a marker of membrane metabolism, lactate (Lac), which is an indicator of ischemia and mobile lipids.

Although, the MRI findings indicate a normal central nervous status in post MTBI, it has been determined by P-MRS that concentrations of the cerebral metabolites mentioned above

Score	Infant (<1 year old)	Child (1-4 years old)	Adult
RESPONSES of EYES			
4	Open	Open	Open
3	To voice	To voice	To voice
2	To pain	To pain	To pain
1	No response	No response	No response
VERBAL RESPONSES			
5	Coos, babbles	Oriented, speaks, interacts, social	Oriented and alert
4	Irritable cry, consolable	Confused speech, disoriented, consolable	Disoriented
3	Cries persistently to pain	In appropriate words, inconsolable	Nonsensical speech
2	Moans to pain	Incomprehensible, agitated	Moans, unintelligible
1	No response	No response	No response
MOTOR RESPONSES			
6	Normal, spontaneous movement	Normal, spontaneous movement	Follow commands
5	Withdraws to touch	Localizes pain	Localizes pain
4	Withdraws to pain	Withdraws to pain	Withdraws to pain
3	Decorticate flexion	Decorticate flexion	Decorticate flexion
2	Decerebrate extension	Decerebrate extension	Decerebrate extension
1	No response	No response	No response

Table 1. Glasgow Coma Score (Teasdale & Jennett, 1974).

change. Several studies with P-MRS have indicated that it is possible to detect neural injury i.e. loss of neuron by comparing these concentrations and the related ratios of pre and post MTBI (Luyten &Den Hollander, 1986; Cecil et al., 1998; Friedman et al., 1998; Friedman et al., 1999; Onbaşlı et al., 1999; Garnett et al., 2000; Brooks et al., 2000; Holshouser, 2000; Garnett et al., 2001; Rao et al., 2006). Whereas death of neurons manifests itself as the deficiency of NAA concentration, the increased Cho concentration is related to the cell membrane breakdown (Brooks et al., 2001). These changes both occur in occipital, parietal and frontal lobes and the splenium of the corpus callosum of brain regions (Ross et al., 1998). The related regions of brain are seen in Figure 5.

In MTBI, the metabolic abnormality is relatively small and due to this reason no lesion in brain tissue is observed in P-MRI results and the related GCS is higher than 14. Moreover, as is known from medical literature, these patients generally exhibit prolonged neurological deficits. In this context, P-MRS is considered as the most sensitive probe for detection of minor changes in brain metabolites. Determination of MTBI has a significant role for both

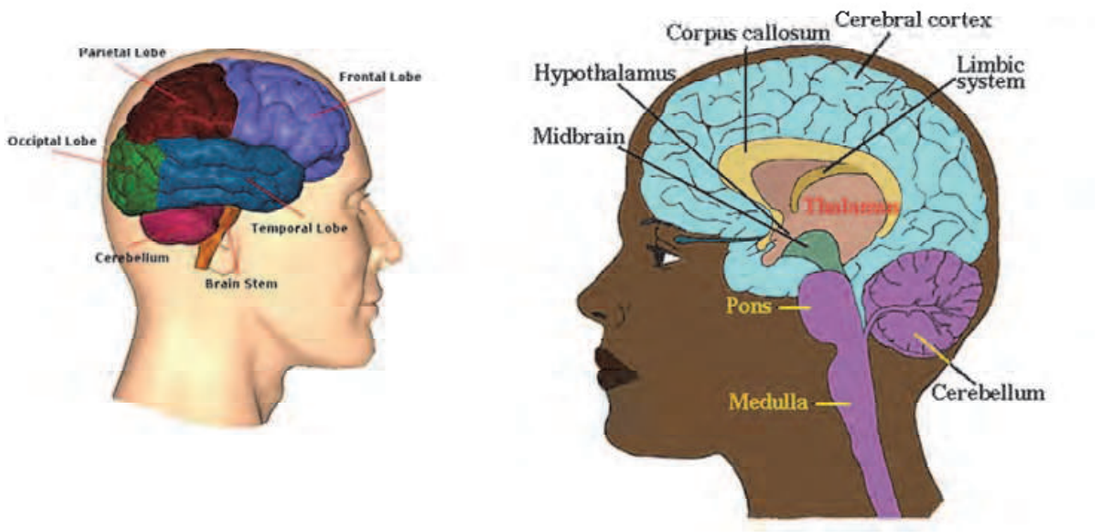

Fig. 5. The brief anatomy of human brain (Royal Adelaide Hospital web site, 2010; Weber State University web page, 2010).

medical diagnosis about the neuron loss percentage and that for forensic science investigations.

In this context, the MTBI has been investigated via four volunteers experimental subjects[1] (mean age: 25 years old; age range: 23-27 years old; mean weight: 75 kg; sex: male; profession: sportsman) by detection of NAA, Cho and Cr metabolites with P-MRS for pre and post trauma for both corpus callosum splenium and frontal white lobe of brain.

To obtain MTBI, sportsmen performed boxing for five minutes as a practice by using boxing gloves and head guard for protection. All experimental subjects were fully awake according to GCS of "15" for pre and post MTBI. No lesion such as hematoma or ecchymose was viewed in P-MRI experiments in pre and post MTBI. For comparison, MRI photographs of sagittal section for pre and post MTBI of one of the experimental subjects are given in Figure 6 (Eruygun, 1998). The results have been confirmed by professional neurologist that no difference between the images given in Figure 6, which were taken from corpus callosum splenium and frontal white lobe of brain, has been detected before and after minor trauma.

After taking the MRI for post trauma, P-MRS experiments were realized within one and half hour after trauma. Proton single voxel spectroscopy[2] experiments have been performed for corpus callosum splenium and frontal white lobe of brain. The data obtained by pre and post P-MRS experiments are listed in Table 2 for the sections of brain mentioned above.

[1] All volunteers have been informed about the investigation process and they all accepted the experiment.

[2] The single voxel techniques generate a cubic or rectangular shaped volume element i.e. voxel with maximum 8cm^3 volume for a region of the sample with P-MRS. Two pulse sequences are used in P-MRS: The STEAM (STimulated Echo Acquisition Mode) and PRESS (Point RESolved Spectroscopy). Both STEAM and PRESS sequences generate cubic or rectangular shaped voxel by acquisition of three orthogonal slice selective 90^o pulses and 90^o pulse followed by two 180^o pulses, respectively. In the STEAM technique, the signal contamination outside the tissue observed is minimum.

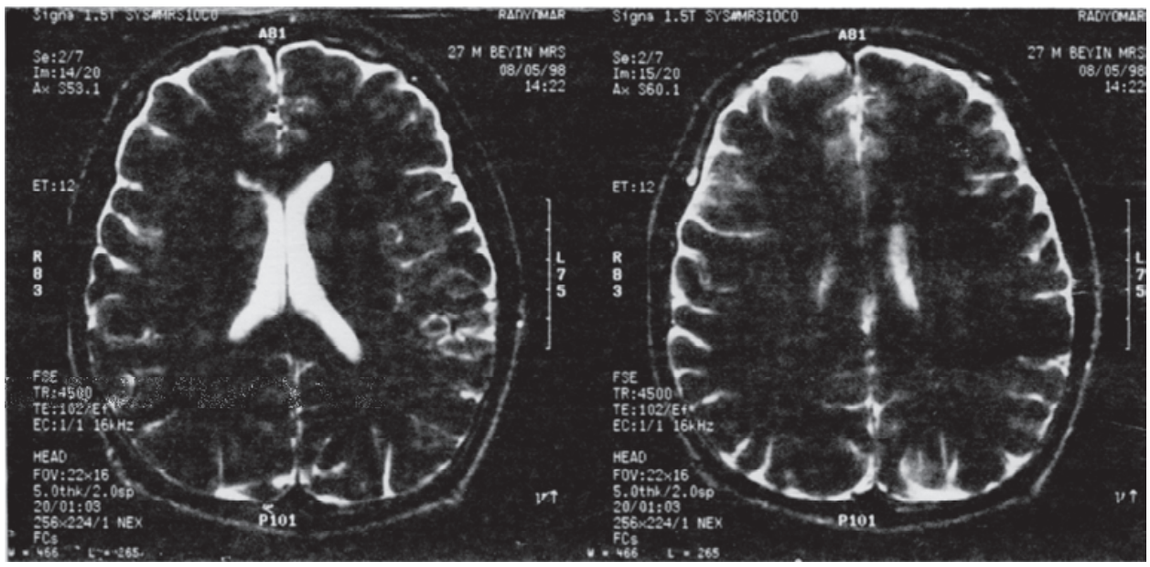

(a) Pre-trauma for sagittal section

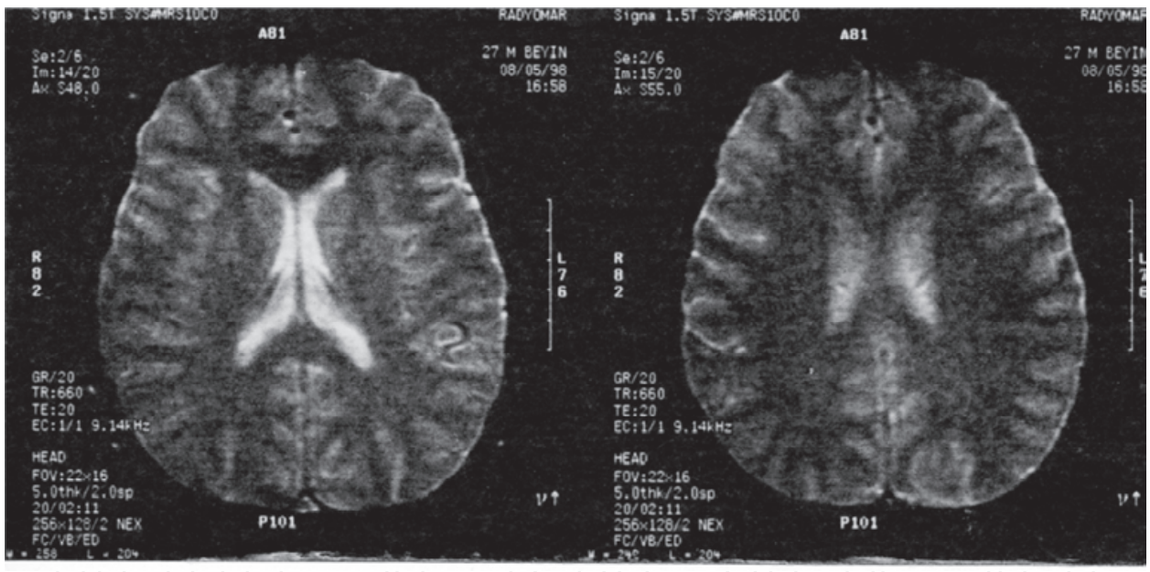

(b) Post trauma for sagittal section

Fig. 6. MRI images of experimental subject 1 for (a) pre trauma and (b) post trauma from sagittal section. MR imaging of these regions were performed by General Electric Signa 1.5T MRI device.

As is seen from Table 2, the neuron marker, NAA, decreases after the minor brain trauma, whereas the replenishing metabolites of Cholin, increases for every lesions of the all volunteers' brain.

The pre and post trauma P-MRS photographs of one of the experimental subject for the both corpus callosum splenium and the white frontal lobe of brain are given in Figure 7 and 8, respectively. The heights of peaks of the metabolites for pre and post trauma are marked on the left and the right of the photographs, respectively.

As is seen from Figure 7 and 8 no pathologic peak has been observed.

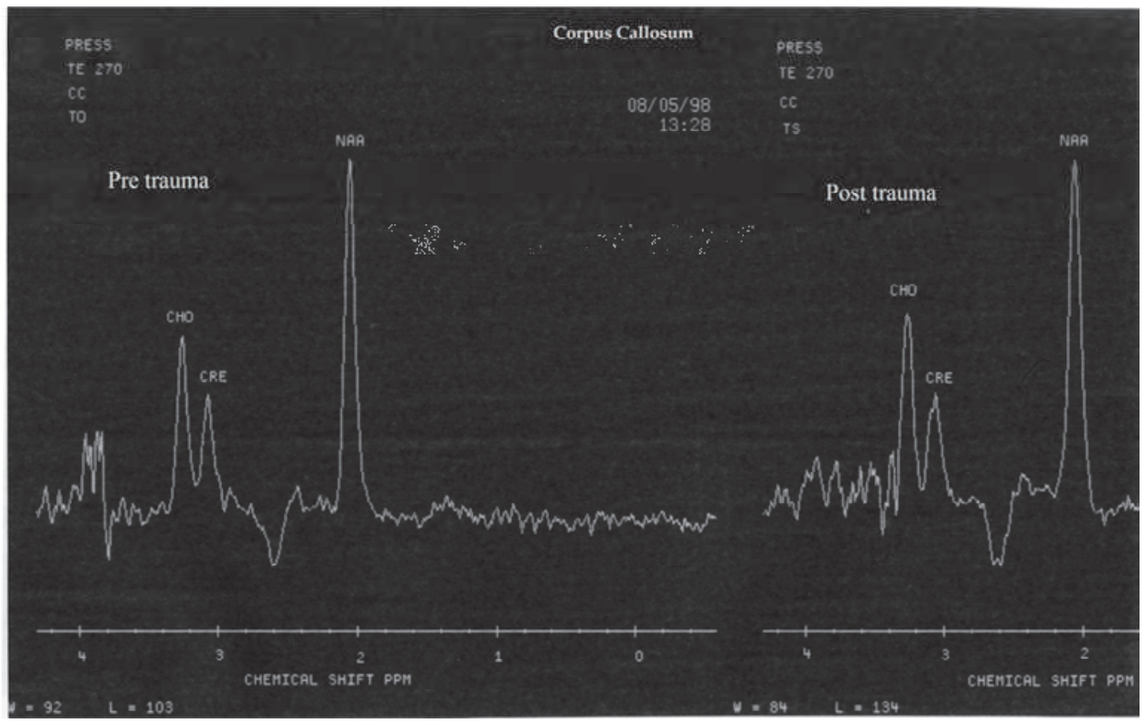

Fig. 7. Brain P-MRS images one of the experimental subject for corpus callosum splenium.

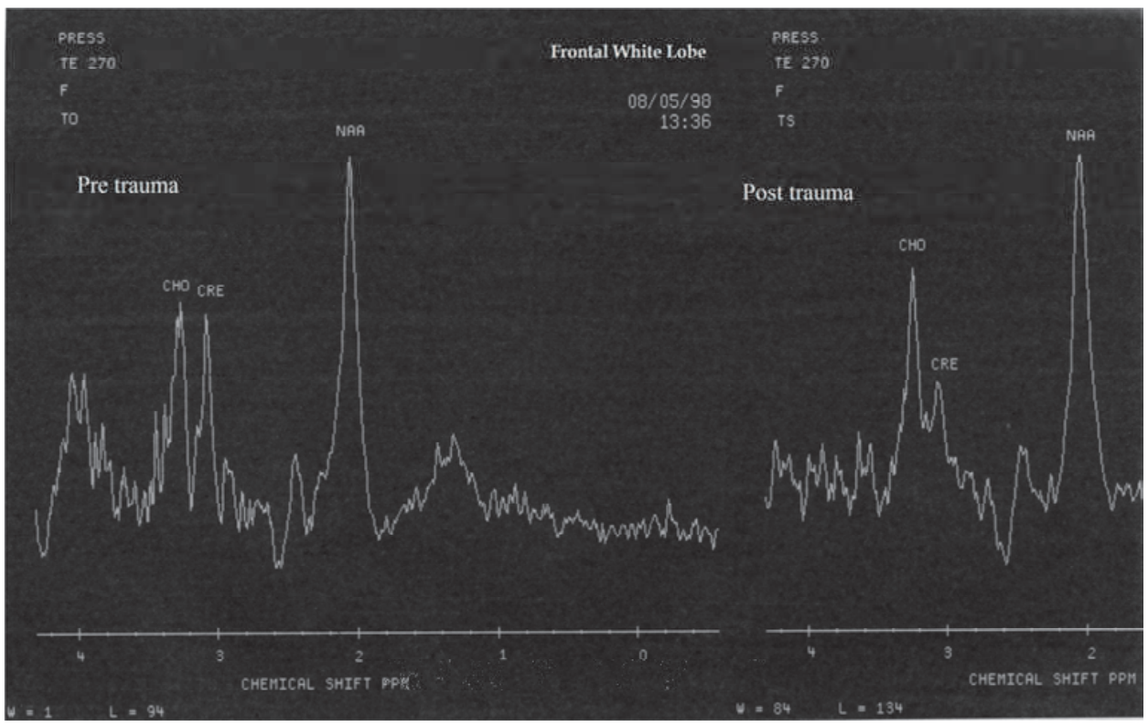

Fig. 8. Brain P-MRS images one of the experimental subject for white frontal lobe.

Brain Sections	Corpus Callosum Splenium Pre trauma			Corpus Callosum Splenium Post trauma			White Frontal Lobe Pre trauma			White Frontal Lobe Post trauma		
Metabolites	NAA	Cr	Cho	NAA	Cr	Cho	NAA	Cr	Cho	NAA	Cr	Cho
Experimental Subject 1	126	46	57	118	34	63	123	42	53	120	47	60
Experimental Subject 2	120	52	47	120	49	73	123	54	52	120	53	84
Experimental Subject 3	128	43	63	122	38	70	129	60	66	123	44	81
Experimental Subject 4	118	42	57	114	40	75	123	46	55	116	61	77

Table 2. By means of chemical shift of metabolites in MRS results for pre and post MTBI (Eruygun, 1998; Onbaşlı et al, 1999).

2.4 Conclusion

The observation of the change in the amplitude of brain metabolites at the vicinity of hydrogen nuclei via P-MRS has been only used for clinical diagnosis for several years. In addition to clinical researches, a new method for determining of closed and mild brain injuries, which are caused due to psychological pressure, beating or any kind of abusing, has been introduced for forensic science investigation for the first time. Moreover, in order to make clear beyond a reasonable doubt for the detection of such mild brain trauma, the P-MRS has been suggested as the most reliable scientific tool for forensic science investigations as well as medical diagnosis.

3. High temperature superconductors as a new terahertz wave sources

Terahertz waves have various advanced technological applications including medical diagnosis, security, biomedical imaging, atmospheric researches, drug and food inspection, gas tracing etc. (Tonouchi, 2007). Terahertz waves also known as T-waves, exist a frequency region between microwaves and far infrared of the electromagnetic spectrum. As is seen from Figure 9, terahertz waves occupy a region from 300 GHz to 10 THz that can provide imaging and sensing technologies not available through conventional technologies such as X-rays.

In recent years, T-waves are extensively utilized for non-destructive security devices since many materials and living tissues are semi-transparent at terahertz wavelengths and also have distinct THz absorption spectra namely “finger prints”. Unlike X-rays, THz radiation posses a little or no health threat since that T-ray photons are both not strong enough to ionize atom or molecules and not able to break the chains of chemical bonds[3]. Moreover, T-waves, especially in 1-10 THz region, have great advantages for biomedical imaging such as tumor recognition, detection of dental cavities etc. due to its non-invasiveness and low Rayleigh scattering property factor compared with optical waves (Lu et. al., 2010). Furthermore, DNA molecules and many proteins have collective vibration and rotation

[3] THz waves have low photon energies (1 THz = 4.1 meV), one million times weaker than X-rays, and do not cause harmful photoionization in biological tissues.

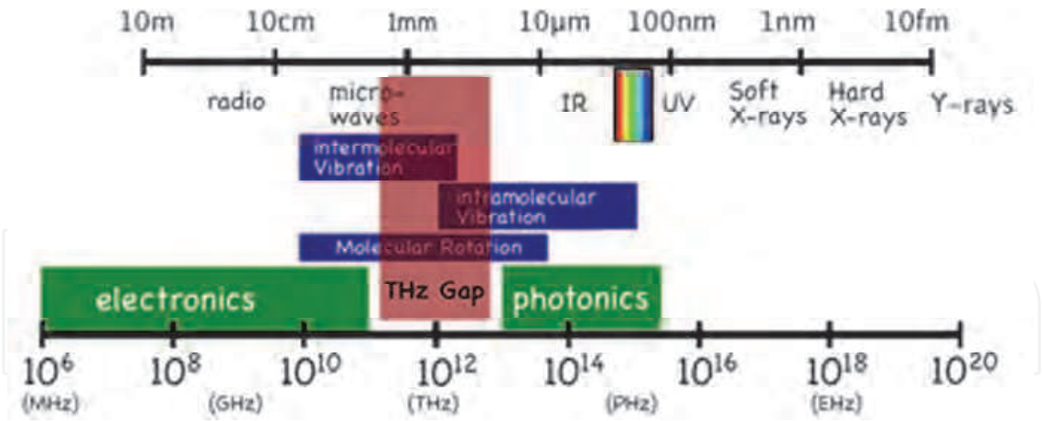

Fig. 9. Terahertz waves in the electromagnetic spectrum (Zomega Terahertz Corp, 2010). The terahertz gap lies between electronics and photonics.

modes that coincide with THz region. Due to this reason, T-waves have also a crucial importance for molecular imaging (Zuhang et.al, 1990; Young et al., 1990; Feng et.al, 1991; Nossal & Lecar, 1991).

There are many ongoing researches for developing terahertz wave sources. One of the most popularly used terahertz wave sources is optoelectronic terahertz wave generators. In this process, near-infrared laser light illuminates a metal-semiconductor-metal structure that results in a photocurrent which is utilized as terahertz wave. Ultrafast fiber lasers and diode lasers & photo-mixers are used for "pulsed" and "continuous wave" sources, respectively. In recent years, the semi-conducting light sources have extended the limit of emission of T-rays to 1.6 THz for quantum cascade lasers and 1.5 THz for unitravelling-carrier photo diodes (Ito et. al. 2005; Walther et. al, 2006). On the other hand, the frequency of alternating currents in semiconductors is limited by finite electron velocities, while that of solid state lasers are limited by thermal energies which prevent the small electronic transition required for lasing at THz wavelengths.

Among the sources mentioned above, superconductors, especially the high temperature superconductors that display "Intrinsic Josephson Effect" (IJE), may be the excellent promising candidate for terahertz source due to their extremely low noise factor and wide frequency coverage (Emuidzinas & Richards, 2004; Güven Özdemir et al, 2009, Moody, 2009). Very recently, continuous and monochromatic terahertz wave emitter with the frequency of 0.63THz has been achieved for the intrinsic Josephson junctions in high temperature $Bi_2Sr_2CaCu_2O_{8+\delta}$ superconductor by applying d.c. voltage in the order of milivolt (Minami et. al. 2009). The voltage due to the fluxon flow mechanism in the system excites the Josephson plasma with terahertz frequency. The frequency of 0.63THz can be considered as the beginning of the filling the THz gap, that is defined between 300 GHz to 10 THz, by high temperature superconducting terahertz sources. The long term goal of the scientists working on that area is to cover the whole THz gap by superconducting coherent terahertz wave sources.

In this chapter, the copper oxide layered mercury based cuprate family superconductors, $HgBa_2Ca_2Cu_3O_{8+x}$, which have the highest Meissner transition temperature of 140K ever obtained at normal atmospheric pressure and display IJE, is proposed as an intrinsic terahertz wave source, since there is no need to apply any bias voltage to the system.

3.1 Mercury cuprates as an intrinsic terahertz wave sources

As is known that the copper oxide layered high temperature superconductors such as $Bi_2Sr_2CaCu_2O_8$, $Tl_2Ba_2Ca_2Cu_3O_{10}$, $HgBa_2Ca_2Cu_3O_{8+x}$ etc. have a common structure in which superconducting copper oxide layers are separated by a thin insulating layer. Copper oxide layers are electromagnetically coupled together by Josephson tunneling process. According to the experimental evidences, cuprates such as $Bi_2Sr_2CaCu_2O_8$, $Tl_2Ba_2Ca_2Cu_3O_{10}$ and $YBa_2Cu_3O_{7-x}$ behave like a stack of superconductor-insulator-superconductor structure i.e. intrinsic Josephson junctions (IJJ) (Kleiner & Müller, 1994; Özdemir et. al, 2006; Güven Özdemir et. al., 2009)

As is known, the main Josephson plasma excitation modes in weakly Josephson coupled layered superconductors are longitudinal (along the c-axis) and transversal (in the ab-plane) plasma modes. Whereas the transverse-mode plasma oscillations can be converted into electromagnetic waves at the boundary of the junctions (Machida & Tachiki, 2001), the longitudinal plasma propagation modes in an array of IJJ do not lead the electromagnetic wave radiation, since the electromagnetic wave has only transverse mode (Bae &Lee, 2006).

Mercury based superconductors have been considered as an array of IJJ. Since, the Interlayer Theory[4] is valid at low temperatures for the optimally oxygen doped mercury cuprates (Özdemir et. al, 2006), all copper oxide layers along the c-axis of the system are in the resonance with the Josephson plasma frequency that coincides to the THz gap (Güven Özdemir et. al, 2007). This type of Josephson plasma resonance mode cannot be attributed to the fluxon flowing mechanism, since the working magnetic field interval never exceeds the lower critical magnetic field of the system. Hence, the magnetic flux is totally expelled from the superconductor. The phenomenon is displayed as a perfect diamagnetic response on SQUID data. Ultimately, the terahertz plasma oscillations determined in the system provide the bulk mercury cuprate superconductor as an intrinsic coherent terahertz wave source without application of any external voltage.

The Josephson plasma frequency values for the mercury cuprates had already been calculated via magnetic critical current density J_c, which was deduced by magnetization versus magnetic field curves obtained by SQUID[5] (Özdemir et. al, 2006; Güven Özdemir et. al., 2009). The Josephson plasma frequency, f_P is calculated via Josephson penetration depth, λ_J .

$$f_P = \frac{c}{2\pi\lambda_J} \tag{1}$$

where λ_J describes the penetration depth of the magnetic field induced by the supercurrent flow in the superconductor. The Josephson penetration depth is defined as

[4] According to Interlayer theory, electron pairing in the superconducting state makes the transport process along the c-axis to be coherent via Josephson (Lawrence-Doniach like) coupling between the superconducting copper oxide layers. Moreover, in order to provide the coherent transport mechanism along the c-axis, the Josephson coupling energy must be equal to the superconducting condensation energy (Anderson, 1997; Anderson 1998).

[5] The critical current density at the vicinity of lower critical magnetic field had already been calculated by Bean critical state model.

$$\lambda_J = \sqrt{\frac{c\phi_0}{8\pi^2 J_c d}} \tag{2}$$

where, c is the speed of light, J_c is the magnetic critical current density, ϕ_0 is the magnetic flux quantum, and d is the average distance between the copper oxide layers (Ferrel & Prange, 1963; Ketterson & Song, 1999; Fossheim & Sudbo, 2004).
We have calculated the intrinsic Josephson plasma frequencies for the optimally and over oxygen doped Hg-1223 superconductors. The related data have been listed in Table 3.

The optimally oxygen doped Hg-1223 superconductors		The over oxygen doped Hg-1223 superconductors	
Temperature (K)	Plasma Frequency, f_p (Hz)	Temperature (K)	Plasma Frequency, f_p (Hz)
4.2	8.303×10^{13}	5	3.295×10^{13}
27	3.363×10^{13}	17	2.175×10^{13}
77	8.303×10^{12}	25	1.981×10^{13}
		77	1.866×10^{12}
		90	1.537×10^{12}

Table 3. The Josephson plasma frequencies for the optimally and over oxygen doped Hg-1223 cuprate superconductors (Özdemir et al., 2006; Güven Özdemir et al., 2007; Güven Özdemir, 2007).

In Figure 10, the Josephson plasma frequency versus temperature curves and the related fitting functions for both the optimally and over oxygen doped $HgBa_2Ca_2Cu_3O_{8+x}$ superconductors are shown.
The temperature dependence functions of the Josephson plasma frequency for the optimally and over oxygen doped Hg-1223 superconductors have been determined by Origin Lab 8.0 graphic program. According to the fitting functions given in Eqs. (3) and (4), an extra doping of oxygen atoms to the optimally doped system changes the temperature dependence of f_P and also lowers the plasma frequencies.

$$f_P(T) = 8.303 \times 10^{12} + \frac{\left(8.303 \times 10^{13} - 8.303 \times 10^{12}\right)}{1 + \left(\frac{T}{21.65914}\right)^3} \tag{3}$$

for the optimally oxygen doped Hg-1223 superconductor

$$f_P(T) = 1.537 \times 10^{12} + \left(3.29503 \times 10^{13} - 1.537 \times 10^{12}\right)\left[\frac{0.5}{1 + 10^{-(11-T)0.05941}} + \frac{1 - 0.5}{1 + 10^{-(15-T)0.05882}}\right] \tag{4}$$

for the over oxygen doped Hg-1223 superconductor

3.2 Brief conclusions for mercury cuprate intrinsic terahertz wave sources

Both the optimally and over oxygen doped mercury cuprate samples exhibit intrinsic terahertz Josephson plasma frequencies at relatively high temperatures. The optimally oxygen doped system starts to emit a coherent terahertz waves at the vicinity of liquid nitrogen temperature of 77K, whereas for the over oxygen doped samples, this effect starts

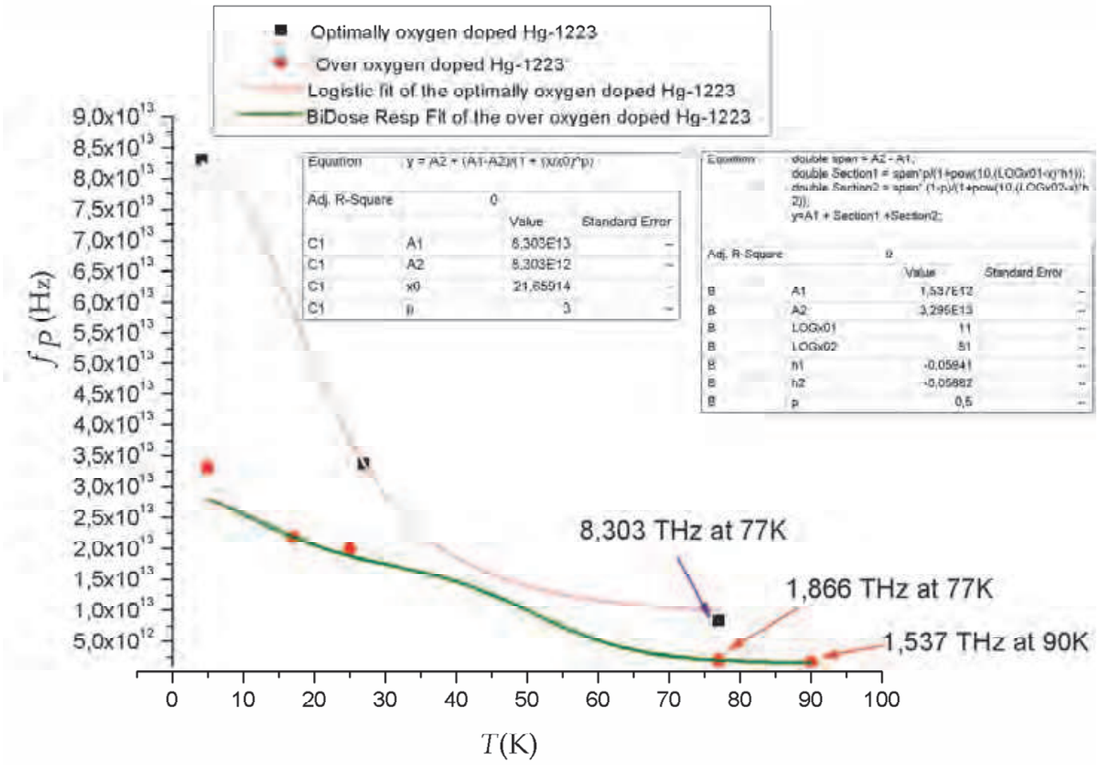

Fig. 10. The intrinsic Josephson plasma resonance frequency versus temperature curves and fitting functions for both the optimally and over oxygen doped mercury cuprates.

above 77K. So it has been concluded that the excess oxygen only affects the starting temperature of emission of coherent terahertz wave in the superconducting system.

4. Intrinsic Quantum Bit "Qubit" operations with mercury cuprate high temperature superconductors

4.1 Introduction to quantum computers and qubit

In recent years, quantum computers have an increasing attention due to their both high speed and memory capacity. As is known that quantum computers are completely different from the classical computers which are based on the standard semiconductor transistor technology. While classical bit is used in the classical computers, the quantum bit namely "qubit", which can carry two quantum states at the same time, is used in the quantum computers. Quantum computers are operated by some quantum mechanical phenomena such as quantum superposition, quantum entanglement and quantum teleportation.

A quantum computer maintains a sequence of qubits. A single qubit is represented by $|0\rangle$, $|1\rangle$ or crucially any quantum superposition of these states. The quantum superposition of these orthogonal states is defined by

$$|\psi\rangle = c_1|0\rangle + c_2|1\rangle \tag{5}$$

The squares of the complex coefficients c_1^2 and c_2^2 represent the probabilities for finding the particle in the corresponding states. Pair of qubits can be in any quantum superposition of 4

(=2^2) states and three qubits in any superposition of 8 (=2^3) states etc. While, for the classical computer one of these states has the probability of "1", for the quantum computer, the sum of the probabilities of these states equals to "1". In this point of view, quantum superposition allows a particle to be in two or more quantum states at the same time. So that the quantum computation is a parallel computation in which all 2^M basis vectors are acted upon at the same time. This parallelism allows a quantum computer to work on a million computations at once, while the desktop PC works on one. A 30-qubit quantum computer would equal the processing power of a conventional computer that could run at 10 **teraflops** (trillions of floating-point operations per second). Today's typical desktop computers run at speeds measured in gigaflops (billions of floating-point operations per second) (Deutchs, 1997). In Figure 11, the difference between classical and quantum computers is illustrated representatively in the context of computation process.

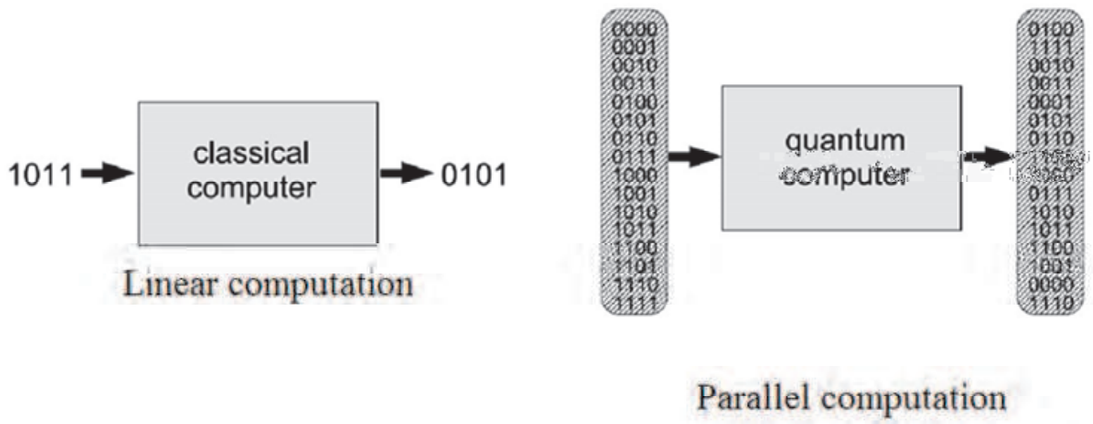

Fig. 11. The main difference between classical and quantum computers by means of computation process (Optical Lattices & Quantum Information Web Site, 2011).

Quantum computers also use a special quantum mechanical phenomenon called as "Quantum Entanglement". In the quantum entanglement, it is possible to link together two quantum particles such as photons or atoms in a special way that makes them effectively two parts of the same entity. Then you can separate them as far as you like, a change in one part is instantly reflected in the other and collectively they constitute a single quantum state (Clegg, 2006). Two entangled particles often must have opposite values for a property, for example, opposite spin. For instance, two photons can be entangled such that if one of them is horizontally polarized, the other is a vertically polarized. It is not important how far they are located, the change in one also reflected in the other. So that quantum entanglement allows particles to have a much closer relationship than is possible in classical physics (Dumé, 2004).
In quantum teleportation, complete information about the quantum state of a particle is instantaneously transferred by the sender to a receiver. This is a great advantage for quantum computing.
In the quantum computers, data is stored by using atoms, photons or fabricated microstructures. In recent years, low temperature superconductors such as Nb and Al have been widely used for qubit technology. Superconducting qubits have an increasing attention due to their collective coherent behavior. As it is well known that the superconducting system can be considered as a condensed state like superfluids so that the all electron pairs

are described by the single quantum state with the quantum wave function, Ψ, which is directly related to the phase difference, φ (Annett, 2004; Clarke & Wilhelm, 2008). In this point of view, this quantum mechanically coherent superconducting system is considered as the most viable for the qubit applications. Furthermore, superconductors provide the general requirement of the quantum circuits such as low dissipation and low noise. The zero resistance phenomenon of the superconducting state provides low dissipation and operating them at low temperatures offers a low noise.

Moreover, the formation of an energy gap between the electron pairs energy states and the free electron energy states has a crucial role in the superconducting qubit technology, since a significant amount of energy is needed for escaping the electron from this collective coherent state. So that it is very difficult to destroy the coherence of the physical superconducting qubit system. The mentioned collective behavior of superconductors that yields to a macroscopic quantum wave function, Ψ is connected to two crucial effects: "Flux quantization" and "Josephson effect" (Mooij, 2010).

Flux quantization is a fundamental quantum phenomenon in which the magnetic field is quantized in the unit of $\Phi_0 = \frac{h}{2e} = 2.068x10^{-15}Tm^2$, flux quantum. The flux quantization also occurs in Type II superconductors between lower (H_{c1}) and upper (H_{c2}) critical magnetic fields since magnetic field begins to penetrate above the lower critical magnetic field of H_{c1} through the superconductor in discrete (quantized) units while the system is still a superconductor.

In the Josephson effect, electron pairs can quantum mechanically tunnel the thin insulating layer due to the phase difference, φ between the adjacent superconducting layers. The supercurrent (I_s) across the Josephson junction, which consists of two superconducting layers separated by thin insulating layer, is directly related to the gauge invariant phase difference, φ.

$$I_s = I_{\max} \sin\varphi \tag{6}$$

where I_{max} represents the maximum current through the Josephson junction. In this situation, no voltage is applied to the junction. If an appropriate dc voltage is applied to the junction, the supercurrent oscillates with a characteristic angular frequency ω (Josephson, 1962).

$$\begin{aligned} &\frac{d\varphi}{dt} = \omega = \frac{2eV}{\hbar} \rightarrow \omega = \frac{2\pi V}{\Phi_0} \\ &I_s = I_{\max} \sin\left(\varphi + \frac{2eV}{\hbar}t\right) \end{aligned} \tag{7}$$

So that any change in the Josephson current results in a finite voltage across the junction. Hence the Josephson junction behaves as a nonlinear inductor.

Since both the phase coherence and long range order are the essence of the Josephson effect, they both play key roles in the qubit technology.

In the present superconducting qubit technology, some low temperature superconducting tunnel junctions have been utilized and their coherence times are around several microseconds while the operating time of qubit is in the order of nano seconds. The coherence times need some improvement. On the other hand, some high temperature superconductors such as Bi-

family superconductors have been tested for qubit operations but they did not give good results due to their high decoherence that results the loss of quantum information.
If one could fabricate a qubit with high temperature superconductors, it would have great advantages such as multiply connected and coupled millions of qubits in the thickness of 1mm. Since some of the high temperature superconductors consist of intrinsic Josephson junction array, there will no need to fabricate a Josephson junction one by one. Moreover, they will operate at significantly high temperatures such at 100K and above so the system will work with very low cost. On the other hand most the copper oxide layered high temperature superconductors such as Bi-family, Y-family superconductors are considered as two-dimensional superconductors due to their high anisotropy. Among other high temperature copper oxide layered superconductors, mercury cuprate family superconductors, $HgBa_2Ca_2Cu_3O_{8+x}$ have remarkable features for the superconducting qubit technology particularly, flux qubit. Due to this reason, in the following section the working principle of the flux qubit will be reviewed. Afterwards, the essential features of the mercury cuprates such as intrinsic Josephson junction structure, occurrence of the Paramagnetic Meissner effect, the electromagnetic wave cavity behavior, occurrence of the spatial resonance and etc. have been discussed in the context of bulk flux qubit. The last section is devoted to determine the required conditions for operating the bulk mercury cuprate superconductors that work as a flux qubit.

4.2 The working principles of flux qubits

Superconducting qubits are classified by comparing the Josephson coupling energy and the charging energy. Josephson coupling energy is defined by

$$E_J = \frac{\Phi_0 I_{\max}}{2\pi} \tag{8}$$

The Josephson coupling energy characterizes the coupling strength between the adjacent superconducting layers. The charging energy is related to the occurrence of the electric field due to the motion of electron pairs in the junction that described as

$$E_C = \frac{(2e)^2}{2C} \tag{9}$$

where C is the capacitance of the junction.
Charging energy is important for small Josephson junctions. In the flux qubit, Josephson coupling energy is significantly larger than the charging energy ($E_J >> E_C$). The phase of the superconducting wave function is more important than the charge. Different value of the total phase change is connected with the different circulating current.
As is known that flux qubit consists of multiple connected Josephson junctions, typically three Josephson junctions (Fig. 12). If the zero magnetic flux is trapped in the qubit loop, the lowest energy is obtained at the zero phase change with zero current. If the magnetic flux quantum is trapped in the qubit loop, the lowest energy is obtained at the phase change of 2π. If half of a magnetic flux quantum is trapped in the qubit loop, the lowest energy is obtained at the phase change of π and the two fluxoid states have equal energies with opposite circulating currents. This is the basis of the working principle of the flux qubit (Mooij et al., 1999).

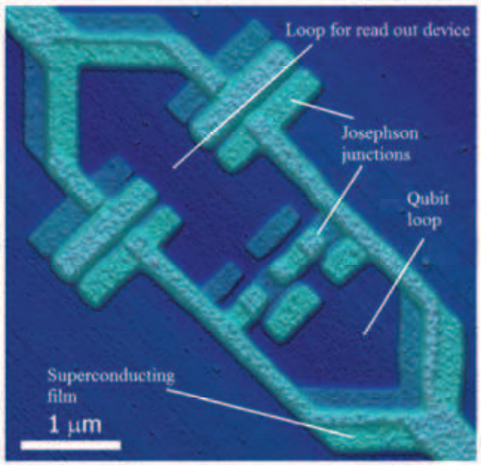

Fig. 12. The configuration of flux qubit consist of three Josephson junctions (Hans Mooij's research group at Delft University of Technology Physics, 2005)

According to Mooij et al., if ($f\Phi_0$) magnetic flux is applied to the qubit loop, where *f* is slightly smaller than 0.5, the system has two stable magnetic-flux states namely $|0\rangle$ and $|1\rangle$ quantum states. As is shown in Fig. 13, one magnetic flux state corresponds to a current, which is the order of several microamperes, of flowing clock wise, the other magnetic flux state corresponds to the same amount of current flowing anti-clock wise (Chiorescu et al., 2003).

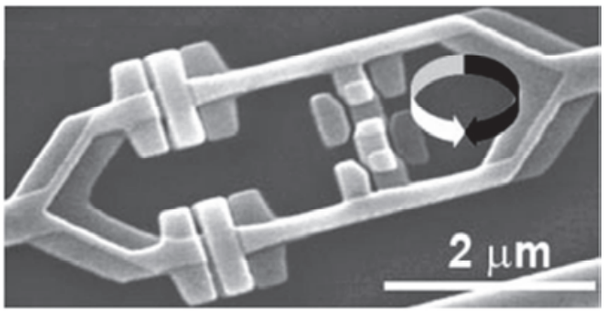

Fig. 13. The Scanning Electron Microscopy (SEM) photography of the micrometer sized superconducting flux qubit. Arrows indicate the clock wise and anti-clockwise currents.

Moreover, the quantum superposition of two states ($|0\rangle$ and $|1\rangle$) is also manipulated by resonant microwave pulses and applying strong microwaves to the system induces hundreds of coherent oscillations. This phenomenon is known as "Rabi oscillations" and it is the basis of quantum gate operations (van der Wal et al., 2000).

One of major problems of superconducting qubits is decoherence which causes the loss of information. Since the phase of quantum wave function dominates the effect of charge in the flux qubit, flux qubit circuits are directly affected by the external flux and its noise that results to cause decoherence (Wellstood et al., 1987; Mooij et al., 1999; Friedman et al., 2000). As is known that quantum information processing is limited by the coherence times. The increasing the coherence time makes possible to carry out a real effective quantum computer in future. From this respect, mercury cuprates have a great potential for flux qubit technology due to their long coherence times as will be expressed in the next section.

4.3 The general properties of mercury based copper oxide layered ceramic superconductors in the context of flux qubit

Besides the fact that the $HgBa_2Ca_2Cu_3O_{8+x}$ cuprate superconductors have the highest Meissner critical transition temperature of 140K at normal atmospheric pressure (Onbaşlı et al, 2009), they have remarkable features for the superconducting flux qubit technology. The crucial advantages of the mercury cuprates have been listed below.

a. **Intrinsic Josephson junction array**: Mercury cuprate family superconductors consist of typical superconducting copper oxide layers which are separated by thin insulating layers. Due to that fact the system is considered as an intrinsic Josephson junction network (Kleiner & Müller, 1994; Özdemir et al., 2006). This property of mercury cuprates removes the problem of the fabrication of the Josephson junctions separately. As is known, in order to build a real quantum computer one needs many coupled qubits. According to the relevant qubit technology, the connected qubit circuits are designed in a special way that allow to 10^5 operations (Mooij, 2010). However, utilizing the bulk mercury cuprate superconductor may increase the number of operation, since the connections between intrinsic Josephson junctions are naturally realized.
b. **The confirmation of interlayer theory and occurrence of spatial resonance**: The interlayer theory, which was proposed by P.W. Anderson for explaining the mechanism of superconductivity in the copper oxide layered high temperature superconductors, has been confirmed for the mercury cuprate family superconductors (Özdemir et al., 2006). According to the interlayer theory of high temperature oxide superconductors, the interlayer coupling correlates electromagnetic coupling along the c-axis with superconducting condensation energy of the superconductor (Anderson, 1997; Anderson 1998). In other words, the Josephson coupling energy equals to superconducting condensation energy in the mercury cuprates at around liquid helium temperature. In this point of view, all superconducting copper oxide layers along the c-axis are in the resonance. Hence, the system behaves like a three dimensional electromagnetic wave cavity. Also it has been determined that the mercury cuprate family superconductors behave like an electromagnetic wave cavity with the frequency of microwave, terahertz and infrared depending on the temperature dealt with (Özdemir et al., 2006; Güven Özdemir et al. 2007; Güven Özdemir et al., 2009).

In this context, the intrinsic Josephson junctions are connected via electromagnetic coupling in the bulk mercury cuprate so that the intrinsic Josephson junctions are in the lossless and perfect communication which has a crucial role in the qubit interactions in quantum computation. Moreover, the spatial microwave electromagnetic wave cavity also is utilized for the manipulation of the quantum states intrinsically.

c. **d-wave symmetric order parameter:** As is known, mercury cuprate superconductors have $d_{x^2-y^2}$-wave symmetric order parameter (Panagapoulos et al., 1996; Panagapoulos & Xiang, 1998; Onbaşlı et al, 2009). According to Taffuri et. al, the qubit proposals basically utilized the fact that the Josephson junctions with a π-shift in phase can be produced by a d-wave order parameter symmetry. This may lead to intrinsically double degenerated system, i.e. systems based on Josephson junctions with an energy-phase relation with two minima (Tafuri et al., 2004). This condition is intrinsically occurs in the mercury cuprate family due to the d-wave symmetry of its order parameter.
d. **Paramagnetic Meissner Effect (PME):** Some superconductors acquire a net positive magnetic moment when they are cooled in weak magnetic fields such as in the order of 1 Gauss. This phenomenon is known as paramagnetic Meissner effect (PME).

Paramagnetic Meissner effect has been observed on both very cleanly prepared some high temperature superconductors and some low temperature superconductors (Braunisch et al., 1992; Braunisch et al., 1993; Schliepe et al., 1993; Khomskii, 1994; Riedling et al., 1994; Thompson et al., 1995; Onbaşlı et al., 1996; Magnusson et al., 1998; Patanjali et al., 1998; Nielson et al, 2000).

Paramagnetic Meissner effect has been observed on both d.c. and a.c. magnetic moment versus temperature data of the mercury cuprate superconductors (Onbaşlı et al, 1996; Onbaşlı et al, 2009). As is seen from Fig. 14, the temperature of T_{PME}, at which the maximum paramagnetic signal is observed on the imaginary component of magnetic moment, is known as PME temperature.

One of the main theoretical explanations of the PME is that the π-junctions between weakly coupled superconducting grains cause spontaneous orbital currents in arbitrary direction. An application of a very weak magnetic field aligns these orbital currents in the opposite direction to diamagnetic Meissner current and hence the system gains a net positive magnetic moment (Braunisch et al., 1992).

The origin of the PME is based on the weakly coupled π-junctions in which the phase difference is π. On the other hand, phase difference is associated with supercurrent of the system. From this respect, the mercury cuprates intrinsically provide the phase change of π which has a key role in the flux qubit as it was mentioned in the previous section.

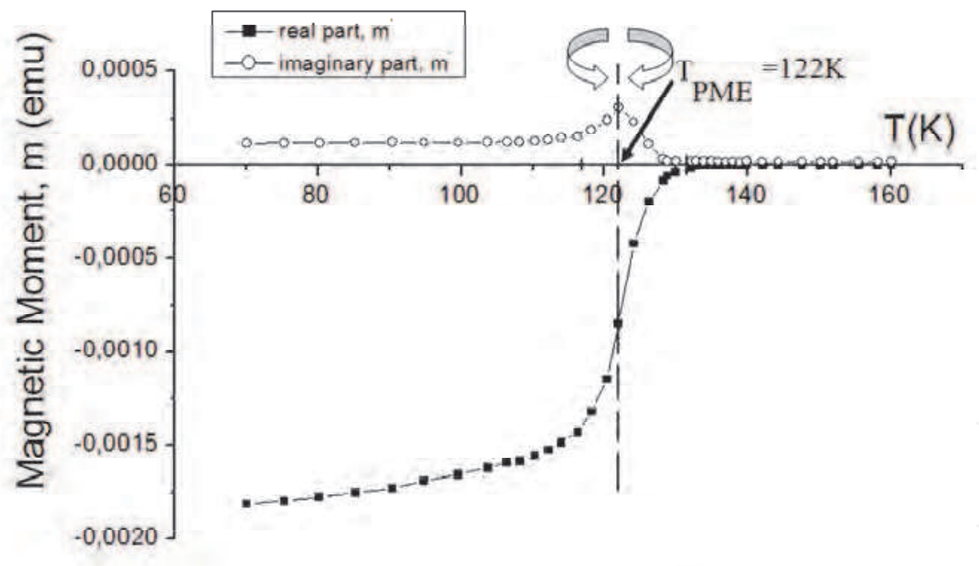

Fig. 14. The a.c. magnetic moment versus temperature data of the optimally oxygen doped mercury cuprates. The data has been taken from the MPMS-5S model quantum design SQUID magnetometer by applying 1 Gauss a.c. magnetic field. The clock wise and anti-clock wise orbital currents both exist at 122K.

As is seen from Fig. 14, for temperatures lower than T_{PME}, the imaginary component of the magnetic moment increases and the orbital current is circulating in one direction clock wise or anti-clock wise. For the temperatures higher than T_{PME}, the imaginary component of the magnetic moment decreases and the orbital current is circulating in the opposite direction to

the previous state. So that at T_{PME} temperature, the clock wise and anti-clock wise currents exist. In this point of view, it has been proposed that the mercury cuprate system can be utilized as an intrinsic bulk flux qubit.

4.4 Concluding remarks on bulk flux qubit character of mercury based copper oxide layered superconductors

As it has been stated in the previous section, the general requirements of the flux qubit are fulfilled by the bulk mercury cuprate superconductors which have been summarized in the following items:

- There is no need to fabricate single Josephson junctions one by one since mercury cuprates intrinsically behaves as a Josephson junction network. Moreover, occurrence of the spatial resonance in the system also forms perfect (lossless) communication between the intrinsic Josephson junctions. In this respect, utilizing mercury cuprates for qubits may increase the present speed of quantum computations.
- There is no need to apply external ($\Phi_0/2$) magnetic flux to the qubit loop to achieve the opposite circulating currents at the same time. As is known that, in order to apply external ($\Phi_0/2$) magnetic flux to the qubit loop, rather complicated, high sensitive and expensive techniques have been used. On the other hand, the existence of opposite circulating orbital currents (clock wise and anti-clock wise) at the same time has been achieved spontaneously by the weakly coupled π -junctions in the mercury cuprates at the T_{PME}.
- In the standard qubit technology, strong microwave pulses have been utilized for manipulating the quantum superposition of these opposite circulating fluxoid states and obtaining the coherent oscillations for quantum gate operations. In this point of view, for qubits produced by the mercury cuprates, the intrinsic microwave cavity behaviour also provides continuous coherent oscillations for the lossless communicated intrinsic qubits in the bulk mercury cuprates.
- One of the main aims of qubit investigations is to fabricate a quantum computer one day. This aim will come true only by obtaining many connected qubits with long coherence times. In this respect, this work may give an insight to obtain a huge number of coupled (lossless communicated) qubits.
- Another important element is that, the opposite circulating orbital currents preserve their state as long as it operates at the temperature of T_{PME}. A remarkable point that the T_{PME} temperature (122K) is approximately 20K below the critical transition temperature of 140K. In this point of view, the required working temperature is very high relative to present low temperature superconducting qubits. In the present superconducting qubit technology, superconducting Aluminum thin films have been extensively used and its critical transition temperature is just 1.2K. So that working with mercury cuprates would lower the cost for technological applications.
- Morever, to fabricate the single intrinsic flux qubit with mercury cuprates is possible by referring to the Scanning Electron Microscopy (SEM) data of the optimally oxygen doped mercury cuprates. The mentioned intrinsic layered structure is shown in Fig.15. The primitive cell of the mercury cuprate contains two intrinsic Josephson junctions in the thickness of approximately 1.5 nm (Aslan et al., 2009). In this context, by using an appropriate technology, it is possible to extract three intrinsic Josephson junctions of about 2.25nm to fabricate single flux qubit with mercury cuprates.

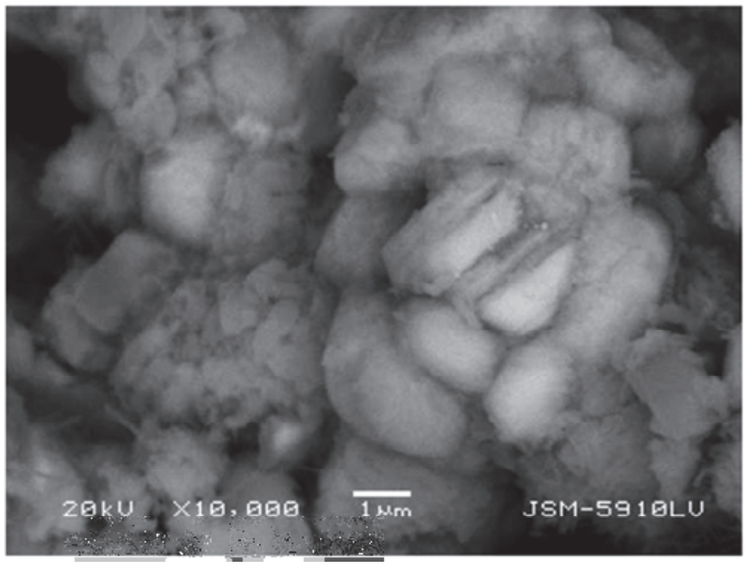

Fig. 15. SEM photography of the optimally oxygen doped $HgBa_2Ca_2Cu_3O_{8+x}$ superconductors. The experiment has been performed JSM-5910 LV Scanning Electron Microscopy.

5. Bolometer applications of high temperature superconductors

Cosmology experiments show that the Universe consists of 73% Dark Energy, 23% Dark Matter and only 4% ordinary matter. The acceleration of the Universe occurs by unknown forces due to the increasing dominance of a mysterious dark energy. In order to resolve the nature of the dark energy and matter, a new generation of telescopes, which are designed to measure the polarization in the cosmic microwave background, is needed. For this kind of telescopes, the advanced detectors called as bolometers are required (Kuzmin, 2006).

The bolometer is a thermal detector, which employs an electrical resistance thermometer to measure the temperature of a radiation absorber. In the bolometer, the higher the energy is absorbed, the higher the temperature will be. The variation of the temperature can be measured via an attached thermometer. Today, in the most bolometers semiconductor or superconductor absorptive elements are used instead of metals. These devices can be operated at cryogenic temperatures, enabling significantly greater sensitivity.

One of the promising devices made of high temperature superconducting materials are edge transition bolometers. Upon the discovery of high temperature superconductors, many studies have been focused on the application of these materials in different types of bolometers for the microwave to infrared wavelength regime. The superconducting bolometers consist of patterned thin or thick superconducting film. Their operation is based on their sharp drop in the resistance, R at their transition temperature, T_c. The detector is kept at a temperature close to the middle of the superconducting transition, where the $^{dR}/_{dT}$ is maximum. The edge transition superconductive bolometers have been investigated in various studies (Skchez et al., 1997; Fardmanesh, 2004; Cámara Mayorgaa et al., 2006).

Photo-mixing devices needed for hot electron bolometers, which have been verified with a superconductor-insulator-superconductor (SIS) mixer, have tremendous potential for various applications such as radio astronomy, terahertz imaging, high-resolution

spectroscopy, medicine, security, and defense (Cámara Mayorgaa et al., 2006). Moreover, it has been reported that the design, fabrication and performance of a high temperature $GdBa_2Cu_30_{7-x}$, superconductor bolometer positioned on a thick silicon nitride membrane. The technological feasibility of this high-Tc superconductor transition edge bolometer investigated could satisfy the requirements of a Fabry-Perot (FP) based satellite instrument designed for remote sensing of atmospheric hydroxyl ion (Skchez et al., 1997). Furthermore, the SQUID readout has been already developed for bolometers such as Cold Electron Bolometer (CEB) (Kuzmin, 2006). In addition to these works, it has been reported that a superconductor-insulator–metal bolometer with microwave readout is suitable for large format arrays (Schmidt et al., 2005).

In this study, the mercury based copper oxide superconductors have been proposed as a sensitive and reliable microwave bolometers to be used for the cosmic researches due to the special effect occurs at the paramagnetic Meissner temperature (T_{PME}) which coincides to the space temperature (Aslan, 2007; Aslan et al.,2009). As was explained in the previous section, the PME is intrinsic property which is observed at the vicinity of TPME=122K for the mercury based cuprate superconductors. At this temperature, clock wise and anti-clock wise orbital currents cancel the noise factor in the system. Moreover, at this temperature, the system emits microwaves intrinsically. Since, the temperature of T_{PME} approximately equals to the space temperature, the system reliably works at the space as an intrinsic microwave bolometers for the investigations of dark energy and dark matter qualitatively. Moreover, the temperature of T_{PME} can be modified by oxygen doping rates which enable us to obtain wider range of bolometric measurements. Furthermore, an alternative method for differential resistivity measurements, observation of change in orbital current has been suggested to detect of dark energy very precisely via PME.

6. References

Anderson, P.W. (1997). *The Theory of Superconductivity in the High-Tc Cuprates*, Princeton University Press, ISBN: 0-691-04365-5, Princeton, New Jersey.

Anderson, P.W. (1998). C-Axis electrodynamics as evidence for the interlayer theory of high temperature superconductivity. *Science*, Vol. 279, No. 5354, (20 February 1998) 1196-1198, ISSN:0036-8075 (Print)

Annett, J.F (2004), *Superconductivity, Superfluids and Condensates*, Oxford University Press, ISBN: 0-19-850755-0 (Hbk), Great Britain.

Ariza, M.; Junqué, C.; Mataro, M., Poca, M.A.; Bargallo, N.; Olondo, M. & Sahuquillo, J. (2004) Neuropsychological Correlates of Basal Ganglia and Medical Temporal Lobe NAA/Cho Reductions in Traumatic Brain Injury. *Arch Neurol* Vol.61, No.4 (April 2004), pp 541-544 ISSN 0375-8540 (Online).

Aslan, Ö. (2007). Investigation of the symmetries and the breakages in relativistic and nonrelativistic regions in high temperature superconductors. PhD Thesis Marmara University Institute of Pure and Applied Sciences, Turkey.

Aslan, Ö.; Güven Özdemir, Z.; Keskin, S.S. & Onbaşlı, Ü. (2009). The chaotic points and XRD analysis of Hg-based superconductors". *Journal of Physics: Conference Series,* Vol 153, Number. 1/ 012002 1-9, ISSN:1742-6596 (online), ISSN:1742-6588 (print)

Bachelard, H. & Badar-Goffer, R. (1993). NMR Spectroscopy in Neurochemistry. Review, *J. Neurochem* Vol.61, No.2, pp. 412-429, ISSN 0022-3042.

Bae M.H. & Lee, H.J. (2006). Progress in THz generation using Josephson fluxon dynamics in intrinsic junctions. *IEICE Trans. Electron*. Vol. E89-C, No. 2, 106-112, ISSN:0916-8516 (Print).

Bayer Schering Pharma Web site, (December 2010), Available from: http://www.diagnostic-imaging.bayerscheringpharma.de/scripts/pages/en/public/modalities/magnetic_resonance_imaging_mri/index.php

Blamire, A.M. (2010) NewCastle University, NewCastle Mangetic Resonance Center Web page, Avaliable from: http://www.ncl.ac.uk/magres/research/brain/

Braunish, W.; Knauf, N.; Kataev, V.; Neuhausen, S.; Grutz, A.; Kock, A.; Roden, B.; Khomskii, D. & Wohlleben, D. (1992). Paramagnetic Meissner effect in Bi high-temperature superconductors. *Physical Review Letters*, Vol. 68, Issue 12 1908-1911, ISSN:1079-7114 (Online), ISSN:0031-9007 (Print).

Braunish, W.; Knauf, N.; Bauer, G.; Kock, A.; Becker, A.; Freitag, B.; Grutz, A.; Kataev, V.; Neuhausen, S.; Roden, B.; Khomskii, D. & Wohlleben, D. (1993). Paramagnetic Meissner effect in high-temperature superconductors. *Physical Review B, V*ol. 48, Issue 6 4030-4042, ISSN:1550-235X (Online), ISSN:1098-0121 (print),

Brooks, W.M; Stidley, C.A.; Petropoulos, H.; Jung, R.E.; Weers, D.C.; Friedman, S.D.; Matthew A. Barlow, M.A. Sibbitt Jr., W.L. & Yeo, R.A. (2000). Metabolic and Cognitive Response To Human Traumatic Brain Injury: A Quantitative Proton Magnetic Resonance Study. *J Neurotrauma* Vol.17, No.8 (August 2000), pp. 629–640, ISSN 1557-9042 (Online).

Brooks, W.M.; Friedman, S.; Gasparovic, C. (2001). Magnetic Resonance Spectroscopy In TBI. *J. Head Trauma Rehabil*, Vol.16, No.2, pp. 149-164, ISSN 1550-509X (Online).

Cámara Mayorgaa, I. ; Muñoz Pradas, P.; Michael, E. A. ; Mikulics, M.; Schmitz, A. ; van der Wal, P.; Kaseman, C.; Güsten, R.; Jacobs, K.; Marso, M.; Lüth, H. & Kordoš, P. (2006). Terahertz photonic mixers as local oscillators for hot electron bolometer and superconductor-insulator-superconductor astronomical receivers, *Journal Of Applied Physics*, Vol. 100, No.4, 043116/1-4, ISSN:0021-8979.

Cecil, K.M.; Hills E.C.; Sandel, M.E.; Smith D.H.; McIntosh, T.K. ; Mannon, L.J.; Sinson, G.P.;. Bagley, L.J.; Grossman, R.I. & Lenkinski, R.E. (1998). Proton Magnetic Resonance Spectroscopy For Detection Of Axonal İnjury In The Splenium Of The Corpus Callosum Of Brain-Injured Patients. *J* Neurosurg, Vol. 88, No.5, (May 1998), pp. 795–801, ISSN 1933-0693 (Online).

Chiorescu, I.; Nakamura, Y.; . Harmans, C.J.P.M & Mooij, J.E. (2003). Coherent quantum dynamics of a superconducting flux qubit, *Science*, Vol. 299, No. 5614, 1869-1871, ISSN: 0036-8075 (Print).

Clarke, J. & Wilhelm, F.K. (2008). Superconducting quantum bits. *Nature* Vol. 453, No. 7198, (19 June 2008), 1031-1042, ISSN:0028-0836.

Clegg, B. (2006). *The God Effect: Quantum Entanglement, Science's Strangest Phenomenon*, St. Martin's Griffin, ISBN-10: 0-312-34341-8, USA.

Danielsen, E.R & Ross, B. (1999). *Magnetic Resonance Spectroscopy Diagnosis of Neurological Diseases*, Marcel Dekker Inc, ISBN 0-8247-0238-7, USA.

Deutchs, D. (1997). *The Fabric of Reality: The Science of Parallel Universes--And Its Implications*, Penguin Group, ISBN-13: 978-0-140-14690-5, England.

Dumé, B. (30 June 2004). Entanglement breaks new record. Avaliable from: http://physicsworld.com/cws/article/news/19793

Emuidzinas J. & Richards P.L. (2004). Superconducting Detectors and Mixers for Millimeter and Submillimeter Astrophysics. *Proc. IEEE* Vol. 92, pp.1597–1616, ISSN 0018-9219.

Eruygun, T.O. (1998), Usage of Advanced Superconducting Devices for Forensic Science, Master Thesis Supervised by Ü. Onbaşlı, İstanbul University, Forensic Science Institution.

Fardmanesh, M. (2004). Response analysis and modeling of high temperature superconductors edge transition bolometers. In: *High Temperature Superconductivity 2, Engineering materials*, A.V.Narlikar (Ed.), 477-536, Springer-Verlag, ISBN 3-540-40639-5, Germany.

Feng, Y.; Zhuang, W. & Prohofsky, E.W. (1991). Calculation of Temperature Dependence of Interbase Breathing Motion of a Guanine-Cytosine DNA Double Helix With Adenine-Thymine Insert. *Phys. Rev. A* Vol. 43, No. 2 pp. 1049–1053, ISSN 1094-1622 (Online).

Ferrell R. & Prange R. (1963). Self field of Josephson tunneling of superconducting electron pairs. *Physical Review Letters*, Vol. 10, No. 11, 479-481, ISSN:1079-7114 (Online).

Fishbine, B. (Spring 2003). SQUID Magnetometry, In: *Los Alamos National Laboratory Web Site* (December 2010), Avaliable from: <http://www.lanl.gov/quarterly/q_spring03/meg_helmet_measurements.shtml>

Fossheim, K. & Sudbo, A. (2004) *Superconductivity: Physics and Applications*, John Wiley & Sons, Ltd, ISBN-10: 0-470-84452-3, Great Britain.

Frahm, J.; Bruhn, H.; Gyngell, M.L.; Merboldt, K.D.; Hänicke, W. & Sauter, R. (1989). Localized High-Resolution Proton NMR Spectroscopy Using Stimulated Echoes: Initial Applications To Human Brain *In Vivo. Magn. Reson. Med. Vol. 9, No.1, (January 1989), pp.79-93, ISSN 1522-2594 (Online).*

Friedman, J.R.; Patel, V.; Chen, W.; Tolpygo, S.K. & Lukens, J.E. (2000). Quantum superposition of distinct macroscopic states. *Nature* Vol. 406, No. 6791, 43-46, ISSN: 0028-0836.

Friedman, S.D.; Brooks, W.M.; Jung , R.E.; Chiulli, S.J.; Sloan, J.H.; Montoya, B.T.; Hart, B.L. & Yeo, R.A. (1999). Quantitative Proton MRS Predicts Outcome After Traumatic Brain İnjury. *Neurology* Vol.52, (April 1999), pp. 1384–1391, ISSN 1526-632X (Online).

Friedman, S.D.; Brooks, W.M.; Jung, R.E.; Hart, B.L. & Yeo, R.A. (1998). Proton MR Spectroscopic Findings Correspond To Neuropsychological Function In Traumatic Brain İnjury. *AJNR Am J Neuroradiol,* Vol. 19 No.10, (November/December 1998), pp. 1879–1885, ISSN 1936-959X (Online).

Garnett, M.R.; Blamire, A.M.; Corkill, R.G.; Cadoux-Hudson, T.A.; Rajagopalan, B. & Styles, P. (2000). Early Proton Magnetic Resonance Spectroscopy In Normal-Appearing Brain Correlates With Outcome In Patients Following Traumatic Brain İnjury. *Brain* Vol.123, No.10, (October 2010), pp.2046–2054, ISSN 1460-2156 (Online).

Garnett, M.R.; Corkill, R.G.; Blamire, A.M.; Rajagopalan, B.; Manners, D.N.; Young, J.D.; Styles, P. & Cadoux-Hudson, T.A.D. (2001). Altered Cellular Metabolism Following

Traumatic Brain Injury: A Magnetic Resonance Spectroscopy Study. *J Neurotrauma* Vol.18, No.3, (March 2001), pp. 231–240 ISSN 1557-9042 (Online).

Georgia State University (n.d.) Web site (December 2010), Avaliable from: <http://hyperphysics.phy-astr.gsu.edu/hbase/nuclear/mri.html>

Govindaraju, V.; Gauger, G.E.; Manley, G.T.; Ebel, A.; Meeker, M. & Maudsley, A.A. (2004). Volumetric Proton Spectroscopic Imaging of Mild Traumatic Brain Injury. *AJNR Am J Neuroradiol* Vol.25, (May 2004), pp. 730-737, ISSN 1936-959X (Online).

Güven Özdemir Z.; Onbaşlı, Ü. & Aslan, Ö. (2007). Calculation of microwave plasma oscillation in high temperature superconductors. In: *The Seventh International Conference on Vibration Problems ICOVP 2005 Springer Proceedings in Physics*, E. İnan & E. Kırış (Eds.), 377-382, Springer, ISBN: 978-1-4020-5400-6, Dordrecht, The Netherlands.

Güven Özdemir, Z. (2007). Determination of Electrical and Magnetic Properties of Mercury Based CuO_2 Layered Superconductors. PhD Thesis Marmara University Institute of Pure and Applied Sciences, Turkey.

Güven Özdemir, Z.; Aslan, Ö. & Onbaşlı, Ü. (2009). Terahertz oscillations in mercury cuprate superconductors. *Pramana-Journal of Physics* Vol.73, No.4 pp. 755-763, ISSN 03044289.

Güven Özdemir, Z. (2011). Chaotic Point Works as Qubit in High Temperature Superconductors, *Journal of Applied Functional Analysis (JAFA)* Vol. 6 No 2, pp 165-172, ISSN 1559-1948 (Print) 1559-1956 (Online).

Hans Mooij's research group at Delft University of Technology, (2005). Avaliable from: http://www.physorg.com/news4996.html

Holshouser, B.A.; Ashwal, S.; Shu, S.; Hinshaw, D.B. Jr. (2000). Proton MR Spectroscopy In Children With Acute Brain Injury: Comparison Of Short And Long Echo Time Acquisitions. *J Magn. Reson Imaging* Vol.11, No. No.1, pp. 9–19, ISSN 1522-2586 (Online).

Ito, H..; Nakajima, F.; Furuta, T. & Ishibashi, T. (2005). Continuous THz-wave generation using antenna-integrated uni-travelling-carrier photodiodes. *Semicond. Sci. Technol* Vol. 20 No. 7, S191-S198, ISSN: 0268-1242 (Print).

Josephson, B.D. (1962). Possible new effects in superconducting tunneling. *Physics Letters*, Vol. 1 No. 7, (1 July 1962) 251-253, ISSN: 0375-9601.

Ketterson, J. B. & Song S. N. (1999) *Superconductivity*, Cambridge University Press, ISBN:0-521-56295-3, United Kingdom.

Khomskii, D. I. (1994). Wohlleben effect (Paramagnetic Meissner effect) in high-temperature superconductors, *Journal of Low Temp. Physics*, Vol. 95, No. 1-2 205-223, ISSN: 0022-2291.

Kleiner, R. & Müller, P. (1994). Intrinsic Josephson effects in high-T_c superconductors, *Phys. Rev. B*, Vol. 49,No. 2, 1327-1341, ISSN: 1098-0121 (Print).

Kuzmin, L. (2006) Optimal Cold-Electron Bolometer with a Superconductor-Insulator-Normal Tunnel Junction and an Andreev Contact, 17th International Symposium on Space Terahertz Technology TH3-5, 183-186.

Lu, J.Y; Chang, H.H.; Chen, L.J.; Tien, M.C. & Sun, C.K. (2010). Terahertz-Wave Molecular Imaging Based on a Compact High-Efficiency Photonic Transmitter.

http://gra103.aca.ntu.edu.tw/gdoc/93/D91941004a.pdf

Luyten, P.R. & Den Hollander, J.A. (1986). Observation of Metabolites In The Human Brain By MR Spectroscopy. *Radiology* Vol.161, No.3, (December 1986), pp. 795-798, ISSN 1527-1315.

Machida M. & Tachiki M. (2001). Terahertz electromagnetic wave emission by using intrinsic Josephson junctions of high-Tc superconductors. *Current Appl. Phys.* Vol. 1, No.4-5, 341-348, ISSN: 1567-1739.

Magnusson, J. ; Papadopoulou, E.; Svedlindh, P. & Nordblad, P. (1998). Ac susceptibility of a paramagnetic Meissner effect sample, *Physica C*, Vol. 297, No:3-4, (10 March 1998) 317-325, ISSN:0921-9601.

Minami, H.; Kakeya, I. ; Yamaguchi, H.; Yamamoto, T. & Kadowaki, K. (2009). Characteristics of terahertz radiation emitted from the intrinsic Josephson junctions in high-*T*c superconductor $Bi_2Sr_2CaCu_2O_{8+\delta}$. *Appl. Phys. Lett*. Vol. 95, No. 23 232511/1- 3, ISSN:0003-6951 (Print).

Moody, N.A. (2009). New Waves: Solid State THz Source, Los Alamos National Laboratory, Avaliable from: http://www.lanl.gov/science/ldrd/LDRD-Day-2009/posters/Moody.pdf

Mooij, J.E. ; Orlando, T.P.; Levitov, L.; Tian, L.; . van der Wal, C. H. & Lloyd S. (1999). Josephson persistent current qubit , *Science* Vol .285, no 5430, 1036-1039, ISSN: 0036-8075 (Print).

Mooij, H. (2010). Superconducting qubits: quantum mechanics by fabrication Avaliable from: ftp://ftp.cordis.europa.eu/pub/ist/docs/fet/qip2-eu-29.pdf

National High Magnetic Field Laboratory, Magnet Lab web site, (2010), Avaliable from: http://www.magnet.fsu.edu/education/tutorials/magnetacademy/magnets/page5.html

Nielsen, A. P.; Cawthorne, A.B.; Barbara, P.; Wellstood, F.C.; Lobb, C.J.; Newrock, R.S. & Forrester, M.G. (2000). Paramagnetic Meissner effect in multiply-connected superconductors, *Physical Review B*, Vol. 62, No.21 14380-14383, ISSN: 1550-235X (Online).

Nossal, R. & Lecar, N. (1991*). Molecular & Cell Biophysics*, Perseus Books, ISBN-10: 0201195607, Cambridge, MA.

Onbaşlı, Ü. ; Wang, Y.T.; Naziripour, A.; Tello, R.; Kiehl, W. & Hermann, A.M. (1996). Transport properties of high Tc mercury cuprates. *Physica Status Solidi B* Vol. 194, 371-382, ISSN: 0370-1972

Onbaşlı Ü.; Eruygun, T.O. & Dinçer, A. (1999), Sensitive Usage of Proton MRS in Forensic Medicine, *4th European Conference on Applied Superconductivity*, Sitges, Spain.

Onbaşlı , Ü. ; Güven Özdemir, Z. & Aslan, Ö. (2009). Symmetry breakings and topological solitons in mercury based d-wave superconductors. *Chaos, Solitons & Fractals* Vol. 42, No. 4, (30 November 2009) 1980-1989, ISSN:0960-0779 (Online).

Optical Lattices and Quantum Information web site (2011). Avaliable from: http://olaqui.df.unipi.it/beginners.html

Özdemir, Z.G.; Aslan Ö. & Onbaşlı Ü. (2006). Determination of c-axis Electrodynamics Parameters of Mercury Cuprates. *Journal of Physics and Chemistry of Solids*, Vol.67 No.1-3 (January-March 2006) pp. 453-456 ISSN 0022-3697.

Panagopoulos, C.; Cooper, J.R.; Peacock, G.B.; Gameson, L.; Edwards, P.P.; Schmidbauer, W. & Hodby, J.W. (1996). Anisotropic magnetic penetration depth of grain-aligned $HgBa_2Ca_2Cu_3O_{8+\delta}$. *Phys. Rev B*, Vol. 53, No. 6, R2999-R3002, ISSN: 1098-0121 (Print).

Panagopoulos, C. & Xiang, T. (1998). Relationship between the superconducting energy gap and the critical temperature in high-Tc superconductors. *Physical Review Letters*, Vol. 81, 2336–2339, ISSN: 1079-7114 Online), ISSN: 0031-9007 (Print).

Patanjali, P. V. ; Seshu Bai, V.; Kadam, R.M. & Sastry, M.D.(1998). Anomalous microwave absorption in GdBCO powder: π–junctions and the paramagnetic Meissner effect. *Physica C*, Vol. 296, No. 3-4, (20 February 1998) 188-194, ISSN:0921-4534.

Rao, V.; Spiro, J.; Degoankar, M.; Horská, A.; Rosenberg, P.B.; Yousem, D.M.; Barker, P.B. & Phil, D. (2006), Lesion Location in Depression Post Traumatic Brain Injury Using Magnetic Resonance Spectroscopy: Preliminary Results From a Pilot Study. *Eur. J. Psychiat*. Vol.20, No.2, pp. 65-73, ISSN 0213-6163.

Riedling, S. ; Brauchle, G. ; Lucht, R.; Röhberg, K.; Löhneysen, H.V.; Claus, H.; Erb, A.& Müler-Vogt, G.(1994). Observation of the Wohlleben effect in $YBa_2Cu_3O_{7-\delta}$ single crystals. *Physical Review B*, Vol. 49, No.18 13283-13286, ISSN: 1550-235X (Online).

Ross, B.D.; Ernst, T.; Kreis, R.; Haseler, L.J.; Bayer, S.; Danielsen, E.; Blüml, S.; Shonk, T.; Mandigo, J.C.; Caton, W.; Clark, C.; Jensen, S.W.; Lehman, N.L.; Arcinue, E.; Pudenz R. & Shelden, C.H. (1998). 1H MRS In Acute Traumatic Brain Injury. *J. Magn Reson Imaging,* Vol.8, No.4 (July/August 1998), pp. 829–840, ISSN 1522-2586 (Online).

Royal Adelaide Hosptital web site, (2010), Avaliable from: http://www.rah.sa.gov.au/birs/bi_brain.php

Salibi, N.M. & Brown, M.A. (1998) *Clinical MR Spectroscopy: First Principles*, Wiley-Liss Inc., ISBN-10: 0-471-18280-X, USA.

Schliepe, B.; Stindtmann, M.; Nikolic, I. & Baberschke, K. (1993). Positive field-cooled susceptibility in high-Tc superconductors. *Physical Review B*, Vol. 47, No. 13 8331-8334, ISSN: 1550-235X (Online).

Schmidt, D. R.; Clark, A. M.; Duncan, W. D.; Irwin, K. D.; Miller, N.; Ullom, J. N. & Lehnert, K. W. (2005). A superconductor-insulator-normal metal bolometer with microwave readout suitable for large-format arrays, *Appl. Phys. Lett*. Vol. 86, No. 5, 053505/1-3, ISSN:0003-6951 (Print).

Skchez, S.; Elwenspoek, M.; Gui, C. ; de Nivelle, M.J.M.E. ; de Vries, R.; de Korte, P.A.J.; Bruijn, M.P.; Wijnbergen, J.J.; Michalke, W.; Steinbeie, E.; Heidenblut, T. & Schwierzi, B. (1997). A high-Tc superconductor bolometer on a silicon nitride membran, In: *Micro Electro Mechanical Systems, Proceedings, IEEE MEMS '97*, 506-511, Print ISBN: 0-7803-3744-1

Tafuri, F.; Kirtley, J.R.; Lombardi, F.; Bauch, T.; Il'ichev, E.; Miletto Granozio, F.; .Stornaiuolo, D & Scotti di Uccio, U. (2004). Flavours of Intrinsic d-Wave Induced Effects In $YBa_2Cu_3O_{7-\delta}$ Grain Boundary Josephson Junctions, In Institute of Physics Conference Series Number 181: Proceedings of the Sixth European Conference on Applied Superconductivity, A Andreone, G.P. Pepe, R. Cristiano &G. Masullo (Eds.), 273-282, IOP Publishing, United Kingdom.

Teasdale, G. & Jennett, B. (1974). Assesment of Coma and Impaired Consciousness: A Practical Scale" *Lancet*, Vol.2, No.7872, (13 July 1974), pp. 81-84, ISSN 0140-6736.

Thompson, D.J.; Minhaj, M.S.M.; Wenger, L.E. & Chen, J.T. (1995). Observation of paramagnetic Meissner effect in niobium disks. *Physical Review Letters* Vol. 75, No.3 529-532, ISSN: 1079-7114 (Online).

Tonouchi, M. (2007). Cutting-Edge Terahertz Technology, *Nature Photonics* Vol. 1 , pp.97-105, ISSN 1749-4885.

Van der Wal, C. H. ; Haar, A.C.J.T.; Wilhelm, F.K.; Schouten, R.N.; Harmans, C.J.P.M.; Orlando, T.P. ; Lloyd, S. & Mooij, J.E. (2000). Quantum superposition of macroscopic persistent-current states, *Science*, Vol. 290, No. 5492, 773-777, ISSN: 0036-8075 (Print).

Young, L.; Prabhu, V.V. & Prohofsky, E.W. (1990). Prediction of Modes With Dominant Base Roll and Propeller Twist in *B*-DNA Poly(dA)-Poly(dT), *Phys. Rev. A* Vol. 41, No. 12, pp. 7020–7023, ISSN 1094-1622 (Online).

Walther, C.; Scalari, G..; Faist, J. ; Beere, H. & Ritchie, D. (2006). Low frequency terahertz quantum cascade laser operating from 1.6 to 1.8 THz. *Appl. Phys. Lett*. Vol. 89, No. 23 231121/1- 3, ISSN:0003-6951 (Print).

Weber State University web site, (2010), Avaliable from:
http://departments.weber.edu/chfam/2570/Neuro-3.jpg

Wellstood, F.C.; Urbina C. U. & Clarke, J. (1987), Low-frequency noise in dc superconducting quantum interference devices below 1 K. *Appl. Phys. Lett.*, Vol. 50, No. 12, 772/1-3, ISSN:0003-6951 (Print).

Wikipedia, (December 2010), Avaliable from:
<http://en.wikipedia.org/wiki/Magnetic_resonance_imaging>

Zhuang W.; Feng, Y. & Prohofsky, E.W. (1990). Self-Consistent Calculation of Localized DNA Vibrational Properties At A Double-Helix–Single-Strand Junction With Anharmonic Potential. *Phys. Rev. A* Vol. 41, No. 12, pp.7033–7042, ISSN 1094-1622 (Online).

Zomega Terahertz Corp. Web site, (2010), Avaliable from:
http://www.zomega-terahertz.com/what-is-thz.html

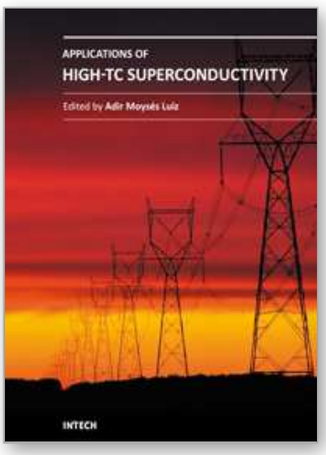

Applications of High-Tc Superconductivity
Edited by Dr. Adir Luiz

ISBN 978-953-307-308-8
Hard cover, 260 pages
Publisher InTech
Published online 27, June, 2011
Published in print edition June, 2011

This book is a collection of the chapters intended to study only practical applications of HTS materials. You will find here a great number of research on actual applications of HTS as well as possible future applications of HTS. Depending on the strength of the applied magnetic field, applications of HTS may be divided in two groups: large scale applications (large magnetic fields) and small scale applications (small magnetic fields). 12 chapters in the book are fascinating studies about large scale applications as well as small scale applications of HTS. Some chapters are presenting interesting research on the synthesis of special materials that may be useful in practical applications of HTS. There are also research about properties of high-Tc superconductors and experimental research about HTS materials with potential applications. The future of practical applications of HTS materials is very exciting. I hope that this book will be useful in the research of new radical solutions for practical applications of HTS materials and that it will encourage further experimental research of HTS materials with potential technological applications.

INTECH
open science | open minds

InTech Europe
University Campus STeP Ri
Slavka Krautzeka 83/A
51000 Rijeka, Croatia
Phone: +385 (51) 770 447
Fax: +385 (51) 686 166
www.intechopen.com

InTech China
Unit 405, Office Block, Hotel Equatorial Shanghai
No.65, Yan An Road (West), Shanghai, 200040, China
中国上海市延安西路65号上海国际贵都大饭店办公楼405单元
Phone: +86-21-62489820
Fax: +86-21-62489821

IntechOpen